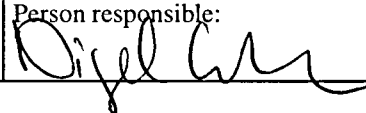


NGU Report 98.064

**Metal and mineral distribution in the Bleikvassli
Zn-Pb deposit, Nordland, Norway**

Report no.: 98.064		ISSN 0800-3416	Grading: Open
Title: Metal and mineral distribution in the Bleikvassli Zn-Pb deposit, Nordland, Norway			
Authors: Terje Bjerkgård		Client: AS Bleikvassli Gruber	
County: Nordland		Commune: Hemnes	
Map-sheet name (M=1:250.000) Mosjøen		Map-sheet no. and -name (M=1:50.000) Korgen	
Deposit name and grid-reference: Bleikvassli - UTM 449030 7312080		Number of pages: 52	Price (NOK): 215
		Map enclosures: None	
Fieldwork carried out:	Date of report: 16.03.1998	Project no.: 2779.00	Person responsible: 
<p>Summary:</p> <p>Studies of metal zonations in the Bleikvassli deposit are important, both for detailed planning of a drilling program and for subsequent interpretations of the results. For this investigation, drillhole data were selected from profiles throughout the deposits at intervals of about 100 meters, except for the old, southern part of the deposit, where all profiles were used because of scarcity of data. The total number of drillcore intersections analysed is 461 and is composed of 1437 individual analyses, representing 1953 meters of drillcore. The data has been weighted according to the lengths of the analyzed intervals and averages of each ore intersection have been calculated.</p> <p>This study show the presence of a pronounced metal zonation in the deposit, with enrichment of copper in the deeper, central part of the deposit, whereas zinc and lead are relatively enriched towards the upper and more northern part of the deposit. This zonation accords with a mineralogical zonation: pyrrhotite ore contains chlorite and/or biotite and is relatively enriched in copper; pyrite ore contains muscovite and/or biotite, and is relatively enriched in zinc and lead. A strong correlation between zinc and lead shows that no major redistribution and separation of these metals took place during the tectonic events affecting the deposit, and that the large-scale zonations observed are likely to be of primary origin. Silver and lead are highly correlated, supporting the view of galena as the main silver carrier in the deposit. Manganese, and to some extent barium, are associated with the copper-rich part of the deposit. This could be a coincidence, due to a primary enrichment in the sediments.</p> <p>Referring to idealized models for SEDEX type deposits, the pyrrhotite-ore enriched in copper could represent the proximal part of the deposit and the pyrite-ore enriched in zinc would be the more distal part. A possibility is that the contact between the Anders Larsa and Kongsfjell Group, which the deposit is very close to, could have been the major pathway for the metalliferous fluids.</p> <p>The distribution patterns presented and maybe especially well visualized in the Cu/Zn-ratio and the distribution of ore/alteration minerals indicate that by going deeper and westwards, the ore might grade into copper-rich impregnations typical of feeder zones, whereas by going northwards the ore might still be rich in zinc and lead. The greatest potential for rich, Zn-Pb ore is therefore towards NW and the deeper levels of the deposit. However structural interpretations are necessary to constrain the potentially best targets.</p>			
Keywords: Bleikvassli	malmgeologi	kobber	
gruve	borkjerneundersøkelse	sink	
Nordland	sonering	sulfid	

CONTENTS

INTRODUCTION.....	5
MODELS FOR METAL ZONATIONS.....	5
THE BLEIKVASSLI DEPOSIT.....	7
DATA BASIS AND HANDLING.....	7
RESULTS.....	9
INTERPRETATIONS.....	11
IMPLICATIONS FOR PROSPECTING.....	13
ACKNOWLEDGEMENTS.....	14
REFERENCES.....	15
TABLES AND FIGURES.....	17

FIGURES

Figure 1: Location of the Bleikvassli Zn-Pb deposit.

Figure 2: Geology in the area around the Bleikvassli deposit (after Rui 1987). The locations of some drillholes are indicated. Also shown is a projection of the ore body to the surface (within dotted blue lines).

Figure 3: A vertical profile of the ore body at 520 N (after Rui 1987).

Figure 4: Schematic models showing typical metal zonations in SEDEX-type and VMS-type sulfide deposits (After Large 1980 and Lydon 1984, respectively).

Figure 5: The Cu/Zn-ratio in drillhole intersections, shown in the XY (North vs. West) and XZ (North vs. Depth) projections. The symbols and values are according to standard deviations from the mean.

Figure 6: The Cu/Zn-ratio in drillhole intersections, shown in the YZ (West vs. Depth) projection. The symbols and values are according to standard deviations from the mean.

Figure 7: The Cu - percentage in drillhole intersections, shown in the XY (North vs. West) and XZ (North vs. Depth) projections. The symbols and values are according to standard deviations from the mean.

Figure 8: The Cu- and Zn-content in drillhole intersections, shown in the XY (North vs. West) projection. The symbols and values are according to standard deviations from the mean.

Figure 9: The Pb- and Ag-content in drillhole intersections, shown in the XY (North vs. West) projection. The symbols and values are according to standard deviations from the mean.

Figure 10: The Zn/Pb-ratio in drillholes, shown in the XY (North vs. West) and XZ (North vs. Depth) projections. The symbols and values are according to standard deviations from the mean.

Figure 11: The Fe-content in drillhole intersections, shown in the XY (North vs. West) and XZ (North vs. Depth) projections. The symbols and values are according to standard deviations from the mean.

Figure 12: Plots of Cu-content versus the Cu/Zn+Pb-ratio and Cu-content versus Zn content in the individual analyzed core intervals and grouped according to mineral assemblages.

Figure 13: The occurrence of various mineral assemblages in drillhole intersections, shown in the XY (North vs. West) and XZ (North vs. Depth) projections.

Figure 14: The Ba- and Mn-content in drillhole intersections, shown in the XY (North vs. West) projection. The symbols and values are according to standard deviations from the mean.

Figure 15: Plots of Mn-content versus Cu-, Zn-, Fe- and Ba-content for the ore intervals in the drillhole intersections (explanations in the text).

Figure 16: Plots of Ba-content versus Fe-content and versus content of base metals for the ore intervals in the drillhole intersections (explanations in the text).

Figure 17: Plots of Mn-content versus Cu-, Fe- and Ba-content and of Ba-content versus Zn-content for ore, alteration and wall rock intersections in cores from profile 360 N (DH 2-90), 520 N (bh. 28-91, bh. 39-93, bh. 9-89, bh.24-91, DH 4-90 and DH 5-90) and 755 N (DH 1-90) (explanations in the text). Data from Moralev et al. 1995.

Figure 18: Ba-content versus Mn-content in drillholes from the profiles 360 N, 520 N and 755 N. The Z-values in the legend is the depth of ore intersections. Data from Moralev et al. 1995.

Figure 19: The content of Zn, Ba and Mn and the Cu/Zn-ratio plotted against depth in the drillholes 1-90, 2-90, 4-90 and 5-90. Data from Moralev et al. 1995.

Figure 20: XY-plots for base metals, Fe and Ag, including all analyzed sections, in the drillholes (N= 1437). For explanations, see text.

TABLES

Table 1 a: Weighted average grades of the Bleikvassli deposit, calculated from the analyzed ore intersections in drillcores.

Table 1 b: Average grades with standard deviations and ranges (not weighted).

Table 2 a: Weighted average grades of the pyrrhotite and pyrite in the Bleikvassli deposit, calculated from the analyzed ore intersections in drillcores.

Table 2 b: Average grades with standard deviations and ranges of the pyrrhotite and pyrite ore (not weighted).

APPENDIX

Tables of weighted averages in the ore intersections in the drill cores.

INTRODUCTION

The sediment-hosted Bleikvassli Zn-Pb deposit is situated in the Rødingsfjell Nappe Complex in the Uppermost Allochthon of the Norwegian Caledonides (Figure 1). It is located in a sequence characterized by muscovite schist, biotite schist, quartz-feldspathic schist, kyanite schist, graphite schist and microcline gneiss. A thick unit of amphibolite is present a few hundred meters below the deposit (Figure 2). This sequence is part of the Kongsfjell Group and the deposit is situated in the upper part of this unit, close to the Anders Larsa Group (Ramberg 1967).

The deposit has been subjected to five phases of deformation of probably both pre-Caledonian and Caledonian age (Bjerkgård et al. 1995, 1997) and a peak metamorphism at middle amphibolite facies (Cook 1993, Spry et al. 1997). The first three phases led to complex isoclinal folding in two stages, followed by formation of large-scale recumbent structures. The two later phases led to gentle flexing of the ore body into partial dome and depression structures. The resulting structures are seen on a vertical profile (Figure 3) and also on the horizontal projection of the ore body to the surface (Figure 2).

Diamond drilling to depths below the known part of the deposit is planned to be carried out during the spring of 1998. Both for detailed planning of this drilling program and for subsequent interpretation of the results, it is important to know if there are systematic variations in metal ratios in the known part of the deposit. Any systematic variations may also give us important clues to the genesis of the deposit.

MODELS FOR METAL ZONATIONS

Both sediment-hosted and volcanic-hosted sulfide deposits are known to show systematic variations in metal content and metal ratios, both vertically and laterally (e.g. Franklin et al. 1981, Lydon 1984, Large 1980, 1983). Sediment-hosted deposits tend to show a lateral zonation to a greater extent when compared to volcanic-hosted deposits (Figure 4). In both cases, chalcopyrite and pyrrhotite are deposited within the feeder system and are important components of the stratiform ore immediately above the feeder zone. Laterally and vertically away from the feeder, the content of sphalerite and galena in the ore increases, whereas the relative modal content of chalcopyrite decreases. Pyrrhotite is also replaced by pyrite. Barite is

formed at the outermost and uppermost parts of the stratiform ore. Laterally away from the deposit, exhalite horizons may be formed, composed of silica, Fe-oxides and/or Mn-bearing phases.

This chemical and mineralogical zonation is mainly a result of a decrease in temperature of the solutions, as well as differences in Eh-pH regimes, as these approach the seafloor and come in contact with the cold sea water (e.g. Lydon 1988). Barite precipitates because Ba combines with sulfate in the sea water; the Fe oxides, Mn-bearing phases and silica are partly formed directly from the low-temperature precipitate derived from the remaining solution and partly from the oxidation of sulfides.

Volcanic-hosted sulfide deposits are very often, but not always, underlain by an extensive and well-defined, zoned alteration halo composed of chlorite-quartz and quartz-sericite (e.g. the Kuroko deposits; Lydon 1984, Løkken; Grenne 1989, Søndre Geitryggen in Folldal; Bjerkgård & Bjørlykke 1994). Not all VMS deposits feature a well-defined alteration zone; recent data indicates that sub-seafloor deposition may be more widespread than previously recognized and characterized by a lack of well-defined alteration (e.g. Middle Valley systems; authors observations). In contrast, sediment-hosted deposits are, in most cases, underlain only by a very weak and subtle alteration zone which may be difficult to distinguish in an intensively metamorphosed and deformed deposit, such as Bleikvassli (Figure 4).

From the above discussion, it is clear that metal zonations and, by implication mineralogical zonations, can be used to define either younging and/or proximal/distal relationships in a deposit (e.g. Cook et al. 1990). In addition to the distributions of sulfides and component metals, the gangue mineralogy and assemblages of alteration minerals can also be used, especially in the case of VMS deposits (Figure 4). However, sulfides such as chalcopyrite, galena and pyrrhotite as well as elements such as Ag, Au, Sb and As are highly mobile during medium to high grade metamorphism and accompanying deformation and may lead to enrichments and dilutions which are superimposed on the primary distributions (e.g. see Vokes 1969, Gilligan & Marshall 1987). Also, mineral transformations (e.g. the formation of pyrrhotite from pyrite) are induced by metamorphism.

THE BLEIKVASSLI DEPOSIT

Three types of sulfide ores are recognized in the Bleikvassli deposit (Vokes 1963). These are 1) massive pyrite ore, 2) massive pyrrhotite ore and 3) mobilizate type veinlets/veins and disseminations, mainly within wallrocks. The pyrrhotite ore is enriched in Cu compared to the pyrite ore, as shown by a Cu/Cu+Pb+Zn-ratio of 0.012 for pyrite ore and 0.085 for pyrrhotite ore (Table 1, Moralev et al. in prep.).

Vokes (1963) suggested that pyrite and pyrrhotite ores represent syngenetic (i.e. primary) compositional variations, noting a zonation from Cu-rich pyrrhotite-ore in the structural footwall to pyrite ore poorer in Cu in the hangingwall in the southern part of the deposit. However, Vokes (op.cit.) also noted several cases of reverse zonation patterns, as well as cases of pyrite ore with pyrrhotite ore on both sides. Skauli (1992) interpreted thin bands of veined pyrrhotite ore as relicts of a primary stringer zone, tectonically displaced from their original position, below the southern part of the ore, where the main bodies of pyrrhotite ore are found. However, Moralev et al. (1995, 1996) considered that most of the chalcopyrite-pyrrhotite ores were actually mobilizates, formed during the later metamorphic events. Cook et al. (in press) also considered the chalcopyrite-pyrrhotite ores to be mobilisates and essentially metamorphogenic in origin. Yet, these authors argued these mobilizates to be largely due to solid-state deformation and thus, distinct from the precious-metal and sulphosalt-rich mobilizates which are considered to be chemical in origin.

The widespread presence of mobilizates shows that redistribution of ore components took place in the Bleikvassli deposit. The mobilizates are enriched in galena, chalcopyrite, fahlore, various Pb-As and Pb-Sb sulfosalts, native Ag and Au and are frequently encountered in the wall rocks, but also within the massive ore itself (Moralev et al. 1995, 1996, Cook et al. in press). The mobilizates form irregular veins and veinlets up to 30-50 cm in thickness and up to tens of meters in length, but are mainly 1-2 cm thick and a few tens of centimeters in extent.

DATA BASIS AND HANDLING

The mine geologists at Bleikvassli have made profiles for every 20 meters across strike throughout the deposit, presenting the geology and location of all drillholes. For this investigation, drillhole data were selected from profiles throughout the deposit at intervals of about 100 meters, except in the old, southern part of the deposit (from -200N to 20N) where

all profiles were used because of scarcity of data. For the rest of the deposit three adjoining profiles 20 meters apart were used in combination to fill any gaps in the profiles.

The analyses are of variable quality because the age span of the analyses ranges from 1950 to 1997. Before 1980, only Cu, Pb, Zn and Fe were analyzed, whereas Ag has been routinely analyzed since 1980. The analyses were done by the mine itself or by SINTEF Mo-Lab in Mo i Rana by XRF. From 1993, the analyses have been carried out by ACME Analytical Labs. Ltd. in Canada, using the ICP-AES technique. Some older cores, especially the long holes drilled from the surface in 1990, were reanalyzed by G.V. Moralev (at ACME and presented in Moralev et al. 1995) and these data have been used in place of the older data.

In total, 1437 analyzed core intervals have been included in this study. For each ore intersection, a weighted average has been calculated, based on the relative length of each core segment analyzed. The resulting number of ore intersections is 461, representing 1953 meters of core. The individual analyzed core segments have also been used in element-element plots, in order to help interpret the map patterns.

The analyses have been checked against the core description logs to be sure that only semi-massive to massive ore has been included and that mobilizates (which typically are strongly enriched in Pb, Ag and Au and have a very low Fe content) are avoided. The analyses of the 461 ore intersections are presented in the appendix.

The Arcview GIS software has been used for data presentations in horizontal (XY or North vs. West) and vertical (XZ or North vs. depth, and YZ or West vs. depth) projections. Because the ore body turns to a more easterly direction around 900 N, (see Figure 2) a new, different, coordinate system has been implemented in this northernmost part of the area, which has an angle of 30° to the old coordinate system. The angle has not been taken into consideration in this work and only 900 N has been added to the coordinates of the old system. In the plots mean and standard deviations from the mean have been used. This is probably the best way of showing anomalies, and values of more than 1 standard deviation from the mean are regarded to be significant.

RESULTS

The weighted average of most of the intervals of the ore intersections provide a representative assay of the deposit as a whole of 0.27 % Cu, 2.72 % Pb, 5.17 % Zn, 45.3 ppm Ag and 205 ppb Au (Table 1). The average content of iron is 16.91 %, showing that the Bleikvassli deposit as a whole consists of a semi-massive ore body.

Plots of the Cu/Zn-ratio (Figure 5 and Figure 6), the Cu % (i.e. $Cu \cdot 100 / (Cu + Pb + Zn)$, Figure 7) and of the Cu-content (Figure 8), show clearly that there are enrichments of Cu in the deeper levels of the deposit and especially between 0 NS and 400 N and at depths below 250 m.a.s.l. There is a big gap in data coverage north of 400 N, but at 600 N the Cu/Zn-ratio as well as the Cu-content is low, showing that the zone of Cu enrichment may either end somewhere between 400 and 600 N, unless it is streaked out westwards and downwards as is indicated by the hole DH 4-90 in profile 520N (1.6 m with 0.55 % Cu, but only 1.65 % Pb, 2.25 % Zn, see appendix). There are also some Cu-enrichments in parts of the Kjøkkenbukta ore body (north of 900N), but the data is too limited at present to recognize trends with any certainty.

The contents of Zn and Pb both increase northwards and are especially high north of 400N (Figure 8 and Figure 9). The contents of Pb are especially high in the area between 400 N and 800 N, whereas Zn is also quite high in the Kjøkkenbukta part of the deposit (i.e. north of 900 N), especially when compared to the area south of 400 N. Pb also shows some enrichments in the older part of the mine, compared to Zn, as is best shown on the plots of the Zn/Pb-ratio (Figure 10). Comparing the plots of Pb and Ag (Figure 9), they are quite similar, inferring that Ag to a large degree follows Pb (see also below).

The content of Fe is the highest in the upper central part of the deposit, that is, between 100 N and 700 N and above 250 m.a.s.l (Figure 11). Thus, the major part of the deposit is actually semi-massive, including some of the most Zn-rich parts (compare Figures 8 and 11).

Mineralogical descriptions exist for about half the ore intersections, including whether it is pyrite-ore or/and pyrrhotite-ore and if the ore contains muscovite, biotite or chlorite (see appendix). The individual analyzed ore intervals have been grouped according to the mineral content, and plots of Cu vs. Cu/Zn+Pb and Cu vs. Zn (Figure 12), show clearly that the pyrrhotite-ore with chlorite and/or biotite in the gangue are enriched in Cu, compared to the

pyrite-ore. Thus, these data support the findings by Vokes (1963), that pyrrhotite ores have the highest Cu content (see also Table 1). This is also seen by calculated averages of the two ore types (Table 2); the pyrrhotite ore contain 0.39 % Cu, 2.14 % Pb, 3.76 % Zn, 49 ppm Ag, 244 ppb Au, whereas the pyrite ore contain 0.18 % Cu, 3.18 % Pb, 6.71 % Zn, 44 ppm Ag and 169 ppb Au.

Plots of the intersections in the XY and XZ planes (Figure 13), show that pyrrhotite-ore with chlorite and/or biotite occurs mainly south of 400 N, whereas pyrite ore with muscovite or/and biotite occurs mainly north of 400 N and to some extent in the upper part, south of 400 N. Unfortunately, no core descriptions with informations about the mineralogy exist for the southernmost and old part of the mine (i.e. south of 0 NS).

The elements Ba and Mn are important since they can be used to discriminate between proximal and distal parts of deposits (see above). Unfortunately, these elements have only been analyzed since 1993, meaning that there are too few data to be truly representative of the entire deposit. The Ba plot (Figure 14), show no clear trends, but there is an indication of higher contents at deeper levels. The plot of Mn content (Figure 14) show a very pronounced Mn enrichment in the deeper parts, south of 400 N. Plotting the Mn content against Cu, Zn, Ba and Fe (Figure 15), show that Mn is correlated with Cu and Fe, but not with Zn and Ba. The map pattern echoes this and confirms that the highest Mn content is associated with the most Cu-rich part of the ore body (compare Figures 8 and 14).

The plots of Ba versus base metals and Fe (Figure 16), show no clear trends, but there are weak indications of a decrease in Ba content with increasing Zn content, and the highest contents of Ba (above 200 ppm) are related to the lowest grade ore.

Moralev et al. (1995) presented new analyses from some of the drillholes in profile 360N, 520N and 755N, including the drillholes 1,2,4 and 5-90, which were drilled from the surface. These analyzed cores included thick sequences of alteration-zone lithologies containing weak mineralizations outside the ore zones (see Moralev et al. 1995 for analysis tables). Plots show that Mn is weakly correlated with both Cu and Fe (Figure 17). In the Cu-Mn plot, there are a number of samples which fall off the trend and have a high Mn-content, but are low in Cu. These samples probably represent a more distal facies. In the Fe-Mn plot, it can be seen that

the Mn-content decreases rapidly when the Fe-content exceeds about 10 %, which shows that Mn is very low in the ore. However, the samples which have the highest Mn-content, also have quite a high Fe-content, which are typical for distal exhalites.

The Ba-Mn plot (*Figure 17*) shows that the samples with the highest Mn-content are also highly enriched in Ba. However, the majority of samples with high Ba-content are low in Mn. The Ba-Zn plot (*Figure 17*) shows that when the Zn-content is higher than about 5000 ppm, the Ba-content decreases rapidly, showing that Ba is very low in the ore. Most of the samples with high Ba-content have a background value of Zn (30-100 ppm) and a low content of Fe (1-7 %) (*Figure 17*). A plot of the Mn versus Ba-content in the individual drillholes (*Figure 18*), show that samples with both high Ba and Mn-content are restricted to the deep intersections in the profiles 360N and 520N. (holes 2, 4 and 5-90).

In *Figure 19*, the analyzes of Ba, Zn, Mn and the Cu/Zn-ratio have been plotted against depth in the drillholes. Except in the ore zones where Ba-bearing minerals are diluted by the large volumes of sulfides, the Ba-content is mainly between 500 and 1000 ppm. These values probably represent background contents or slight enrichments, if compared with averages of the rock types encountered in the drillholes, such as microcline gneiss (540 ppm Ba), garnet-mica schist (675 ppm Ba) and quartz-feldspathic schist (665 ppm Ba, see data compilation in Bjerkgård et al. 1995).

The highest Ba-contents are found in zones enriched in Mn. These zones are present in the profiles for drillhole 2, 4 and 5-90, 10-20 m above the ore zones (*Figure 19*) and in drillhole 5-90, a similar zone is found 50 m below the ore zone. The Mn-content varies from about 1000 ppm to more than 5000 ppm, which are 2-5 times above background values for the lithologies outside the mine area (data in Bjerkgård et al. 1995). The Ba-content varies from 300 to nearly 2000 ppm and several samples have values greater than 1000 ppm, which are also well above background (see above). The core descriptions from these holes identify these zones as very garnet-rich biotite schists, and the Mn is probably present in garnet (e.g. 25.5 to 32.1 % of the spessartine component was found by Cook 1993), whereas Ba is probably incorporated in biotite.

INTERPRETATIONS

This study shows the presence of a very pronounced zonation in the Bleikvassli ore deposit with respect to both mineralogy and metal content. The content of Cu is the highest in the deeper, central part of the deposit, whereas Zn and Pb are relatively enriched towards the upper and more northern part of the deposit. With respect to mineralogy, pyrrhotite-ore with biotite and/or chlorite is mainly present south of 400 N, whereas pyrite-ore with muscovite and/or biotite is present mainly north of 400 N and in the upper parts of the deposit. Thus, Cu enrichments correspond to a large degree to the pyrrhotite ore and relatively higher grades of Zn (and Pb) correspond to pyrite ore.

Plots of Cu-content versus Zn-content and Fe-content, respectively (Figure 20), show that Cu is not correlated with either of the two elements. A plot of Zn versus Fe, on the other hand, shows a good correlation. These patterns correspond well with the observed distribution of Cu and Zn.

The distribution of Zn and Pb show a similar pattern (compare Figures 8 and 9), except that Pb is enriched relative to Zn in the old part of the deposit and in the area between 400 N and 800 N (see also Figure 10). A plot of the Zn- versus Pb-content including all analyzed core intervals show that Zn and Pb are strongly correlated (Figure 20). This shows that, except for the some obvious and generally speaking volumetrically unimportant mobilizates in the wallrocks, no major redistribution and separation of Zn and Pb took place during deformation and metamorphism, at least not on the scale of analyzed intervals (about 10 cm to 2 meters). It is on this basis likely that the enrichments of Pb compared to Zn in parts of the deposit are of primary origin.

The distribution of Ag and Pb in the deposit show a very similar pattern (Figure 9) and a plot of Ag- versus Pb-content for all analyzed core intervals (Figure 20), show that the elements are highly correlated. This supports the view that galena is the main Ag carrier in the Bleikvassli deposit, as has been stated by several other workers (e.g. Eidsmo et al. 1984, Malvik & Pilstrøm 1985, Cook et al. 1997).

If these data now are compared to the idealized models for sulfide deposits and preferentially to the model for zonations in SEDEX type deposits (Figure 4), the pyrrhotite-ore enriched in

Cu would then represent the proximal part of the deposit and the pyrite-ore enriched in Zn would be the more distal part. The presence of chlorite and biotite associated with pyrrhotite ore give support to this interpretation, since these minerals also tend to form in a proximal higher-temperature environment, compared to muscovite which is stable under lower temperature conditions at the peripheries of the system (Riverin & Hodgson 1980).

The presence of a Mn enrichment, and to some extent, also Ba in the proximal part of the deposit does not fit well with the idealized model, as these elements are supposed to precipitate in the very distal part of the deposit, or to cap it (Figure 4). One possibility is that the fluids forming the deposit evolved from a low-temperature, more oxidized, fluid to a higher temperature, more reduced, fluid with time. Another possibility is that the sediments in this part of the strata were originally enriched in Ba and Mn and have nothing to do with formation of the deposit. It could also be that these patterns are a statistical artifact and might be very different if the data were calculated on a sulfide-free basis, thus avoiding the not inconsiderable dilution effects. It should also be noted that large parts of the deposit has not been analyzed for neither Ba nor Mn, which might contribute to the rather ambiguous picture.

IMPLICATIONS FOR PROSPECTING

The Bleikvassli deposit is located very close to the contact between the Anders Larsa and Kongsfjell Group (Figure 2), a contact which might represent a major unconformity. It is possible that the contact is an early formed major fault zone, which marks the contact between the continental platform (the Anders Larsa Group) and the sedimentary basin (the Kongsfjell Group), as was argued for by Bjerkgård et al. (1995, 1997).

Referring again to the idealized model for SEDEX-type deposits, the metalliferous fluids are mainly supplied along a master fault or fault system and the distribution and zonation with respect to metals will therefore be asymmetric, whereas in the case of VMS type deposits a more symmetric pattern is more likely to develop, assuming deposition above the hydrothermal system (Figure 4). If the contact between the two above-mentioned groups does represent a pre-tectonic fault zone, this could therefore also have been the major pathway for the metalliferous fluids. This fits with observed pattern showing a more proximal character going westwards and deeper in the deposit, and thereby also approaching the contact with the Anders Larsa Group.

The distribution patterns presented in the various projections, and perhaps best visualized in patterns shown by the Cu/Zn-ratio (Figure 5) and the distribution of ore/alteration minerals (Figure 13), indicate that by going deeper and westwards, the ore might grade into Cu-rich impregnations typical of feeder zones, whereas by going northwards the ore might still be rich in Zn and Pb. The potential for economic ore could also be considerable further to the south, if tectonic events have sliced off portions of the ore and separated them from the main ore body.

The recommendations based on the observed mineral and metal distributions are that drilling should commence in the area where the potential of finding major Zn-resources are the greatest. According to this work this should be in the area from 500 N and below 200 m.a.s.l. to about 850 N and 0-100 m.a.s.l. Care should be taken to involve interpretations of structures, which could affect the distribution patterns to a significant extent. It is, however, remarkable how straightforward the picture appears on the deposit scale, despite the structural complications, suggesting that a primary zonation pattern has survived subsequent metamorphic and deformational overprinting. The preservation of the macroscopic zonation contrasts with the widespread, local, disruption of zonation patterns noted by most investigators.

It is recommended that in the future drilling programs on the deposit scale the impregnation zones are also analyzed, since they can give more information on the Ba and Mn distribution, as well as it may also contain economic concentrations of precious metals.

ACKNOWLEDGEMENTS

The author greatly acknowledges valuable comments by P.G. Spry, G.V. Moralev and N.J. Cook. N.J. Cook is also thanked for correcting the language.

REFERENCES

- Bjerkgård, T., and Bjørlykke, A., 1994, The stratabound sulphide deposits in the Folldal area, Southern Trondheim Region, Norway: *Norsk Geologisk Tidsskrift*, v. 74, p. 213-237.
- Bjerkgård, T., Larsen, R. B., and Marker, M., 1995, Regional geology of the Okstindene Area, in the Rødingsfjell Nappe Complex, Nordland, Norway: Trondheim, Geological Survey of Norway, 87 pp.
- Bjerkgård, T., Larsen, R. B., and Marker, M., 1997, Regional setting of the Bleikvassli Zn-Pb deposit in Nordland, Norway: *Norges geologiske undersøkelse Bulletin*, v. 433, p. 34-35.
- Cook, N. J., 1993, Conditions of metamorphism estimated from alteration lithologies and ore at the Bleikvassli Zn-Pb-(Cu) deposit, Nordland, Norway: *Norsk Geologisk Tidsskrift*, v. 73, p. 226-233.
- Cook, N. J., Halls, C., and Kaspersen, P. O., 1990, The geology of the Sulitjelma ore field, Northern Norway - some new interpretations: *Economic Geology*, v. 85, p. 1720-1737.
- Cook, N. J., Spry, P. G., and Vokes, F. M., 1997, Mineralogy and paragenetic relationships among sulphosalts and related minerals in the Bleikvassli Zn-Pb-(Cu) deposit, Nordland, Norway: Formation and metamorphism of massive sulphides, Frank M. Vokes 70 year Anniversary symposium, Trondheim, Norway, 1997.
- Cook, N. J., Spry, P. G., and Vokes, F. M., 1998, Mineralogy and paragenetic relationships among sulphosalts and related minerals in the Bleikvassli Zn-Pb-(Cu) deposit, Nordland, Norway: *Mineralium Deposita*, v. 6 - Frank M. Vokes special issue (in press).
- Eidsmo, O., Foslie, G., Malvik, T., and Vokes, F. M., 1984, The mineralogy and recovery of silver in some Norwegian base-metal sulphide ores: The second International congress on applied mineralogy in the minerals industry, Los Angeles, California, february 22-25, 1984, p. 891-910.
- Franklin, J. M., Lydon, J. W., and Sangster, D. F., 1981, Volcanic associated massive sulphide deposits, *in* Skinner, B. J., and Sims, P. K., eds., *Economic Geology*, 75th Anniversary volume, p. 485-627.
- Gilligan, L. B., and Marshall, B., 1987, Textural evidence for remobilization in metamorphic environments: *Ore Geology Reviews*, v. 2, p. 205-229.
- Grenne, T., 1989, The feeder-zone to the Løkken ophiolite-hosted massive sulfide deposit and related mineralizations in the Central Norwegian Caledonides: *Economic Geology*, v. 84, p. 2173-2195.
- Large, D. E., 1980, Geological parameters associated with sediment-hosted, submarine exhalative Pb-Zn deposits: An empirical model for mineral exploration: *Geologische Jahrbuch*, v. D40, p. 59-129.
- Large, D. E., 1983, Sediment-hosted massive sulphide lead-zinc deposits: An empirical model, *in* Sangster, D. F., ed., *Short Course in Sediment-hosted stratiform lead-zinc deposits*: Victoria, Mineralogical Association of Canada, p. 1-26.

- Lydon, J. W., 1984, Ore deposit models 8. Volcanogenic massive sulphide deposits. Part 1: A descriptive model: *Geoscience Canada*, v. 11, p. 195-202.
- Lydon, J. W., 1988, Ore deposit models 14. Volcanogenic massive sulphide deposits. Part 2: Genetic models: *Geoscience Canada*, v. 15, p. 43-65.
- Malvik, T., and Pilstrøm, G., 1985, Occurrence of silver and gold bearing minerals in mill products from some Scandinavian sulphide deposits, *in* Forssberg, K. S. E., ed., *Flotation of sulphide minerals: Netherlands, Elsevier Science Publishers B.V.*, p. 221-237.
- Moralev, G. V., Bjerkgård, T., and Larsen, R. B., 1996, Geology of the Kjøkkenbukta orebody, Bleikvassli Gruber, Nordland, Norway: Trondheim, Geological Survey of Norway, 33 pp.
- Moralev, G. V., Larsen, R. B., and Bjerkgård, T., 1995, Distribution of precious metals in the Bleikvassli Zn-Pb sedex deposit, Nordland, Norway: Trondheim, Geological Survey of Norway, p. 120 pp.
- Ramberg, I. B., 1967, Kongsfjell-området geologi, en petrografisk og strukturell undersøkelse i Helgeland, Nord-Norge: *Norges Geologiske Undersøkelse*, v. 240, 152 pp.
- Riverin, G., and Hodgson, C. J., 1980, Wall-rock alteration at the Millenbach Cu-Zn mine, Noranda, Quebec: *Economic Geology*, v. 73, p. 424-444.
- Rui, I. J., 1991, Diamantboringer ved Bleikvassli gruber i 1990 - Sluttrapport: Oslo, Prospektering A/S, p. 4 pp.
- Skauli, H., 1992, On the formation of Zn-Pb deposits; a case study of the Bleikvassli deposit, Northern Norway. Unpublished thesis, University of Oslo, Norway.: Unpub. Ph.D thesis, University of Oslo.
- Spry, P. G., Rosenberg, J. L., Jacobsen, C. E., Cook, N. J., and Vokes, F. M., 1997, Thermobarometry as applied to the Bleikvassli Zn-Pb-(Cu) deposit, Nordland, Norway: Formation and metamorphism of massive sulphides, Frank M. Vokes 70 year Anniversary symposium, Trondheim, Norway, 1997.
- Vokes, F. M., 1963, Geological studies on the Caledonian pyritic zinc-lead orebody at Bleikvassli, Nordland, Norway: *Norges geologiske Undersøkelse*, v. 222, p. 126 pp.
- Vokes, F. M., 1969, A review of the metamorphism of sulphide deposits: *Earth-Science Reviews*, v. 5, p. 99-143.

TABLES AND FIGURES

Table 1 a: Weighted average grades of the Bleikvassli deposit, calculated from the analyzed ore intersections in drill cores.

Element	Weighted average	Meters of core	Numbers of analyses
<i>Cu %</i>	0.27	1660.04	1294
<i>Pb %</i>	2.72	1660.04	1294
<i>Zn %</i>	5.17	1660.04	1294
<i>Ag ppm</i>	45.3	936.21	554
<i>Au ppb</i>	205	248.7	141
<i>Fe %</i>	16.91	1276.44	967
<i>Co ppm</i>	32	269.9	147
<i>As ppm</i>	355	269.9	147
<i>Cd ppm</i>	127.6	269.9	147
<i>Sb ppm</i>	138	269.9	147
<i>Bi ppm</i>	51	269.9	147
<i>Ba ppm</i>	35	223.6	133
<i>Mn ppm</i>	628	269.9	147

Table 1 b: Average grades with standard deviations and ranges (not weighted).

	Average	Stdev.	Minimum	Maximum	Number
<i>Cu %</i>	0.27	0.25	0.01	2.40	1294
<i>Pb %</i>	2.96	2.12	0.02	13.00	1294
<i>Zn %</i>	5.63	3.50	0.13	26.12	1294
<i>Ag ppm</i>	49.7	60.5	0.8	960.0	554
<i>Au ppb</i>	177	248	5	1765	141
<i>Fe %</i>	19.21	10.41	1.31	55.61	967
<i>Co ppm</i>	30	36	1	240	147
<i>As ppm</i>	285	612	1	4732	147
<i>Cd ppm</i>	153.4	122.5	12.0	836.8	147
<i>Sb ppm</i>	133	251	1	2449	147
<i>Bi ppm</i>	55	44	1	254	147
<i>Ba ppm</i>	57	84	1	587	133
<i>Mn ppm</i>	648	539	110	4825	147

Table 2 a: Weighted average grades of the pyrrhotite and pyrite ore in Bleikvassli deposit, calculated from the analyzed ore intersections in drill cores.

Pyrrhotite ore:

Element	Weighted average	Meters of core	Numbers of analyses
<i>Cu</i> %	0.39	446.55	280
<i>Pb</i> %	2.14	446.55	280
<i>Zn</i> %	3.76	446.55	280
<i>Ag</i> ppm	48.9	393.85	220
<i>Au</i> ppb	244	146.5	77
<i>Fe</i> %	15.03	373.45	211
<i>Co</i> ppm	32	159.2	81
<i>As</i> ppm	299	159.2	81
<i>Cd</i> ppm	112.3	159.2	81
<i>Sb</i> ppm	130	159.2	81
<i>Bi</i> ppm	57	159.2	81
<i>Ba</i> ppm	39	159.2	81
<i>Mn</i> ppm	782	159.2	81

Pyrite ore:

Element	Weighted average	Meters of core	Numbers of analyses
<i>Cu</i> %	0.18	434.98	311
<i>Pb</i> %	3.18	434.98	311
<i>Zn</i> %	6.71	434.98	311
<i>Ag</i> ppm	43.5	353.34	224
<i>Au</i> ppb	169	63.95	44
<i>Fe</i> %	17.47	374.29	269
<i>Co</i> ppm	31	72.45	46
<i>As</i> ppm	365	72.45	46
<i>Cd</i> ppm	158.8	72.45	46
<i>Sb</i> ppm	126	72.45	46
<i>Bi</i> ppm	37	72.45	46
<i>Ba</i> ppm	21	53.65	40
<i>Mn</i> ppm	435	72.45	46

Table 2 b: Average grades with standard deviations and ranges of the pyrrhotite and pyrite ore (not weighted).

Pyrrhotite ore:

	Average	Stdev.	Minimum	Maximum	Number
<i>Cu</i> %	0.39	0.29	0.03	1.79	280
<i>Pb</i> %	2.40	1.90	0.03	11.33	280
<i>Zn</i> %	4.55	3.30	0.36	16.6	280
<i>Ag</i> ppm	52.9	55.1	0.8	471.3	220
<i>Au</i> ppb	202	301	5	1765	77
<i>Fe</i> %	17.36	9.35	3.12	53.87	212
<i>Co</i> ppm	26	33	1	201	81
<i>As</i> ppm	229	525	1	3362	81
<i>Cd</i> ppm	116.7	85.7	11.3	397.1	81
<i>Sb</i> ppm	139	329	1	2449	81
<i>Bi</i> ppm	58	41	5	254	81
<i>Ba</i> ppm	62	84	1	587	80
<i>Mn</i> ppm	836	638	110	4825	81

Pyrite ore:

	Average	Stdev.	Minimum	Maximum	Number
<i>Cu</i> %	0.18	0.18	0.03	2.19	311
<i>Pb</i> %	3.48	2.40	0.04	13	311
<i>Zn</i> %	7.34	4.04	0.556	19.879	311
<i>Ag</i> ppm	49.4	70.8	1.7	960	224
<i>Au</i> ppb	147	158	14.17476	900	44
<i>Fe</i> %	18.41	8.90	3.45	44.23	269
<i>Co</i> ppm	38	40	0.5	240	46
<i>As</i> ppm	231	258	16	1117	46
<i>Cd</i> ppm	202.4	133.5	18	636.9	46
<i>Sb</i> ppm	105	74	16	480	46
<i>Bi</i> ppm	49	43	1	157	46
<i>Ba</i> ppm	30	34	1	124	40
<i>Mn</i> ppm	410	249	121	1107	46

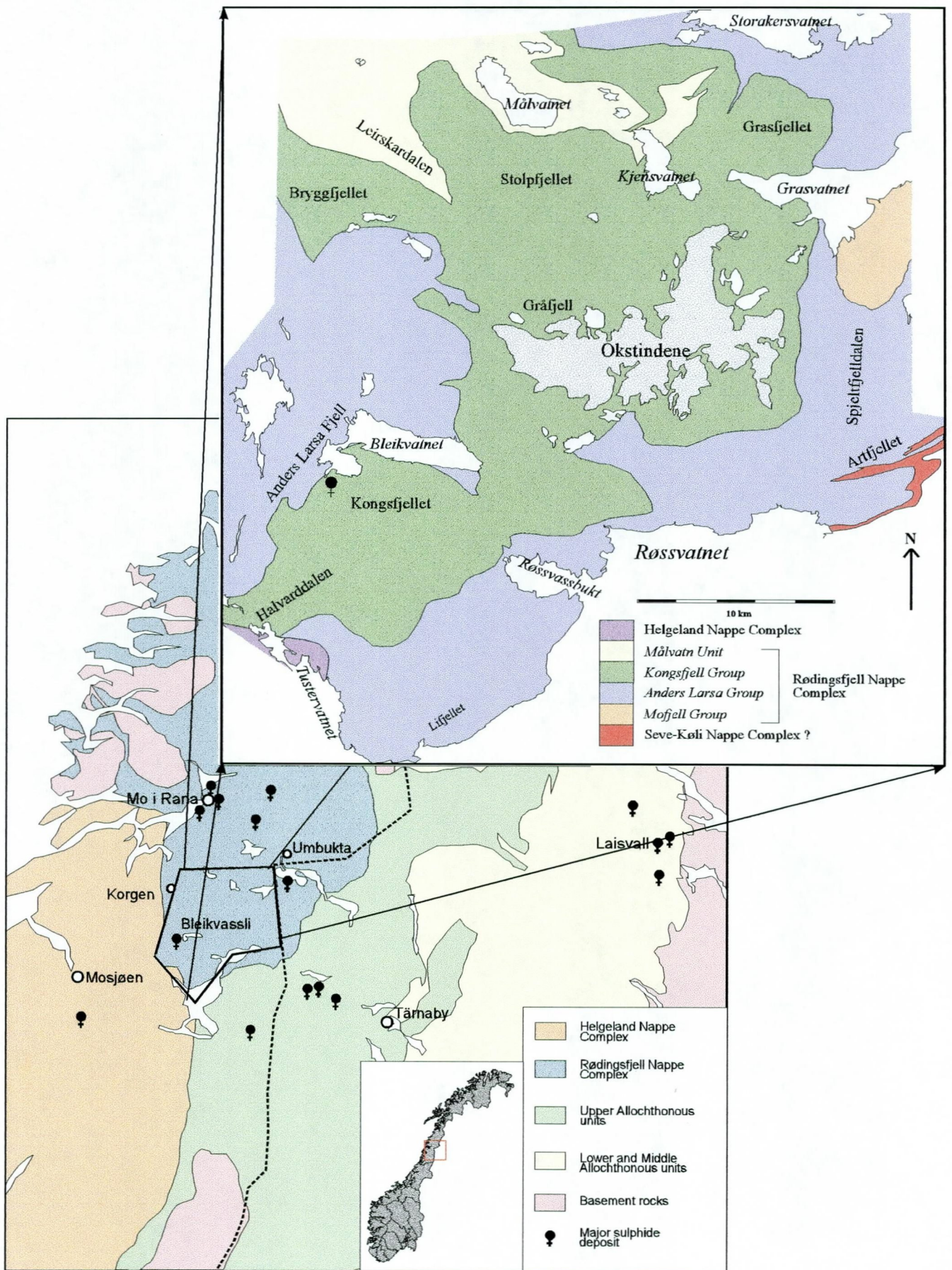


Figure 1: Location of the Bleikvassli Zn-Pb deposit.

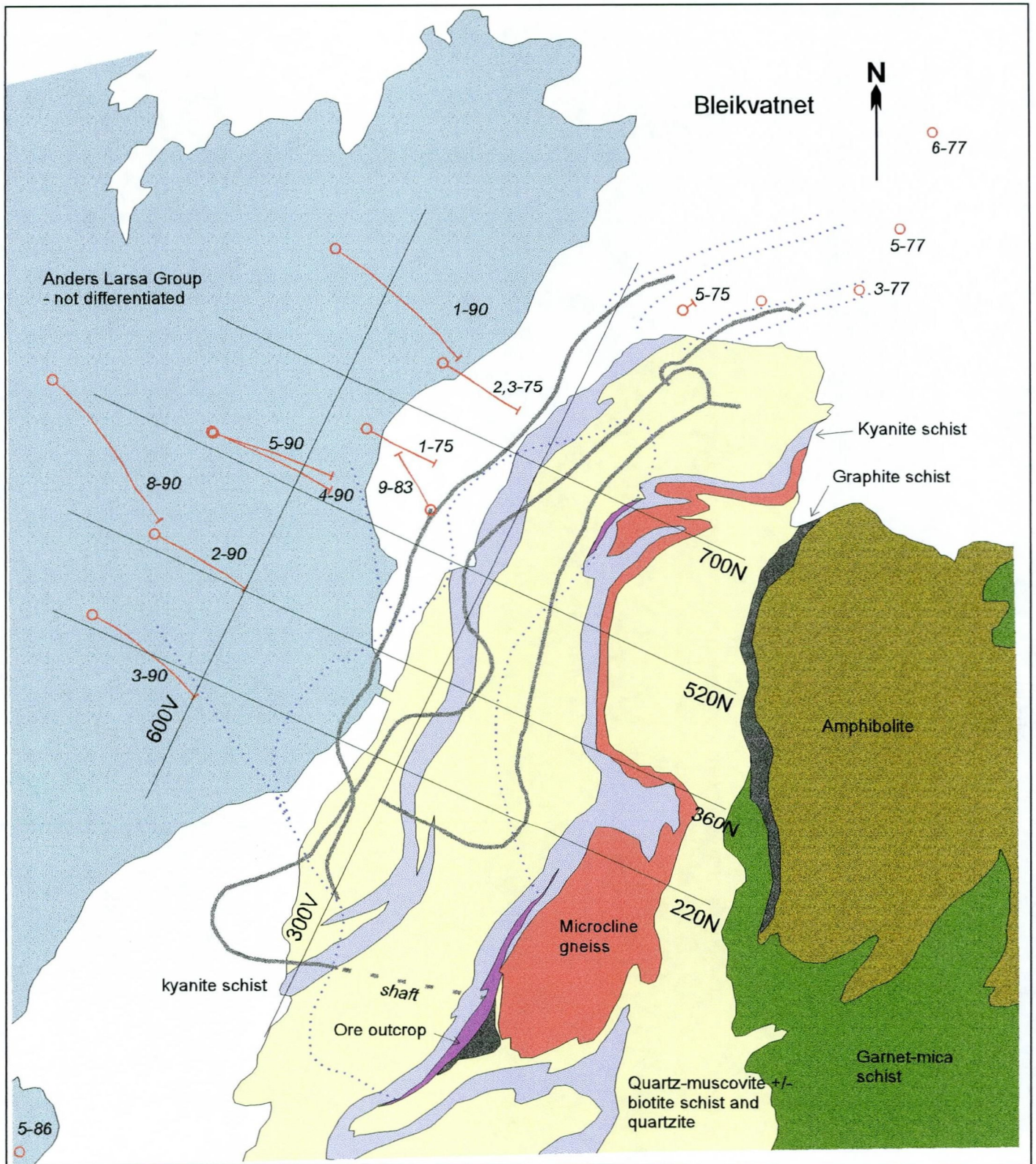


Figure 2: Geology in the area around the Bleikvassli deposit (after Rui 1987). The locations of some drillholes are indicated. Also shown is a projection of the ore body to the surface (within dotted blue lines).

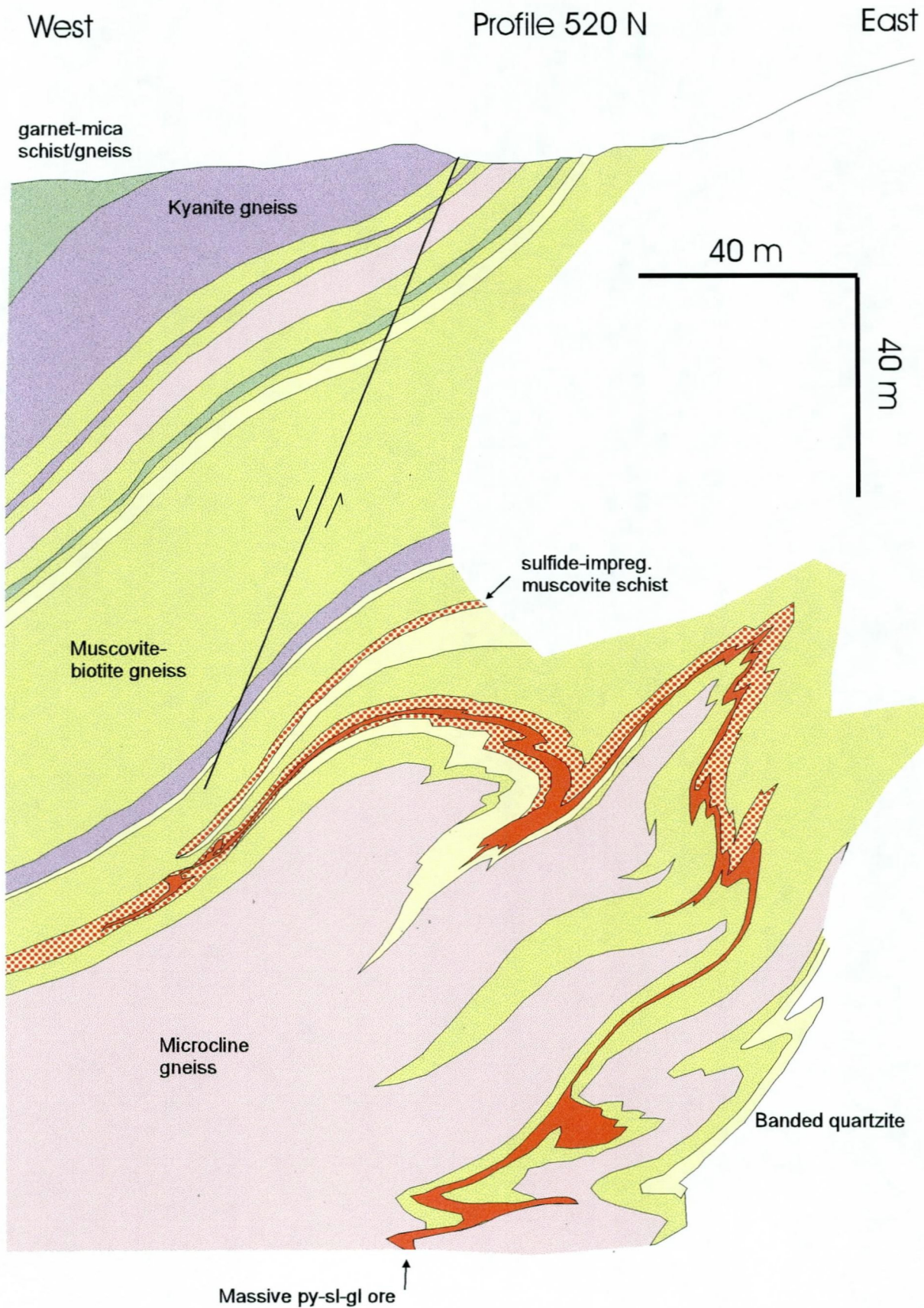
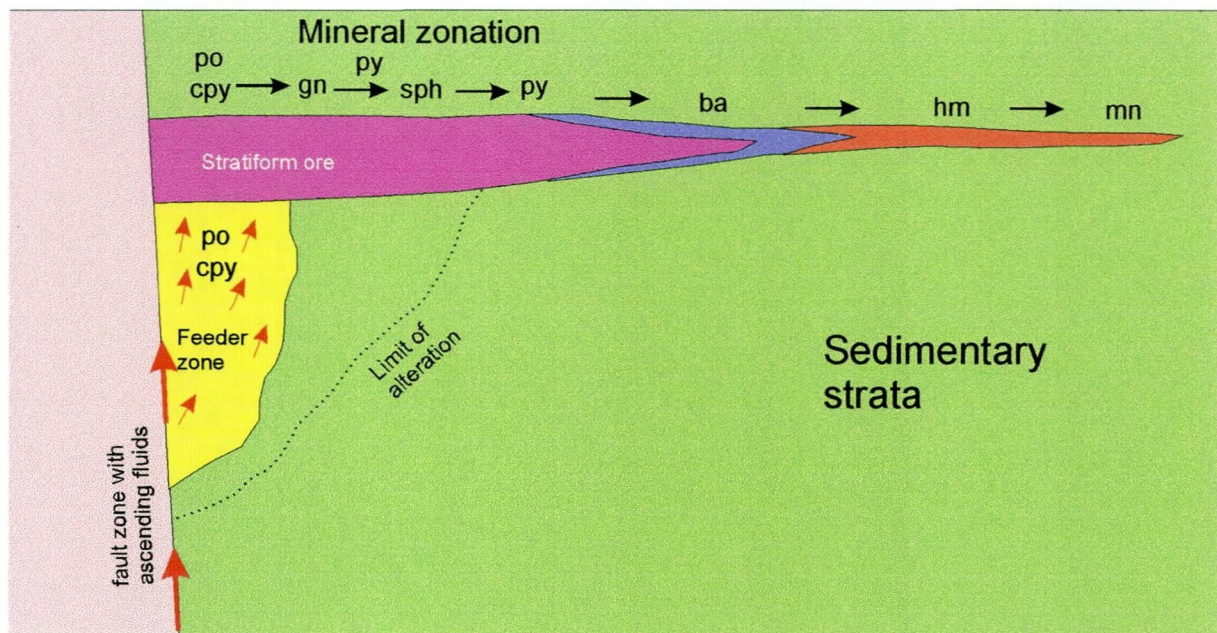


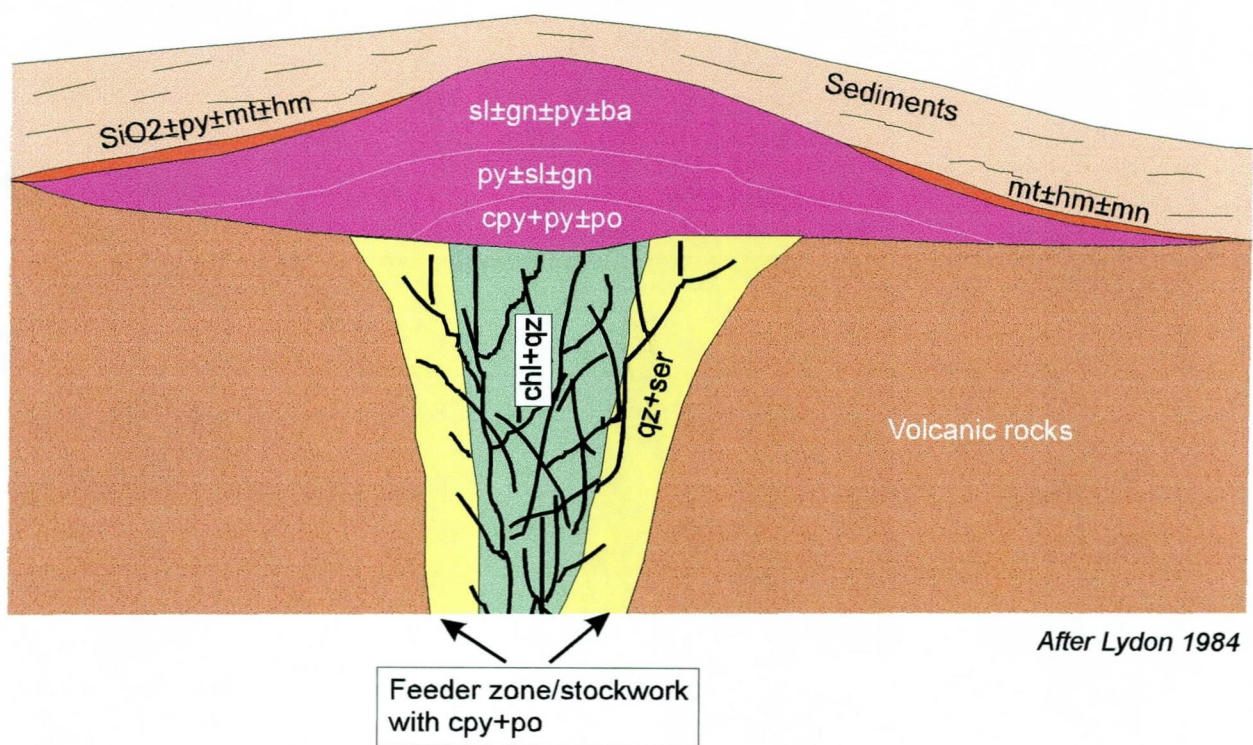
Figure 3: A vertical profile of the ore body at 520 N (after Rui 1987).

Sedex type deposit



After Large 1980

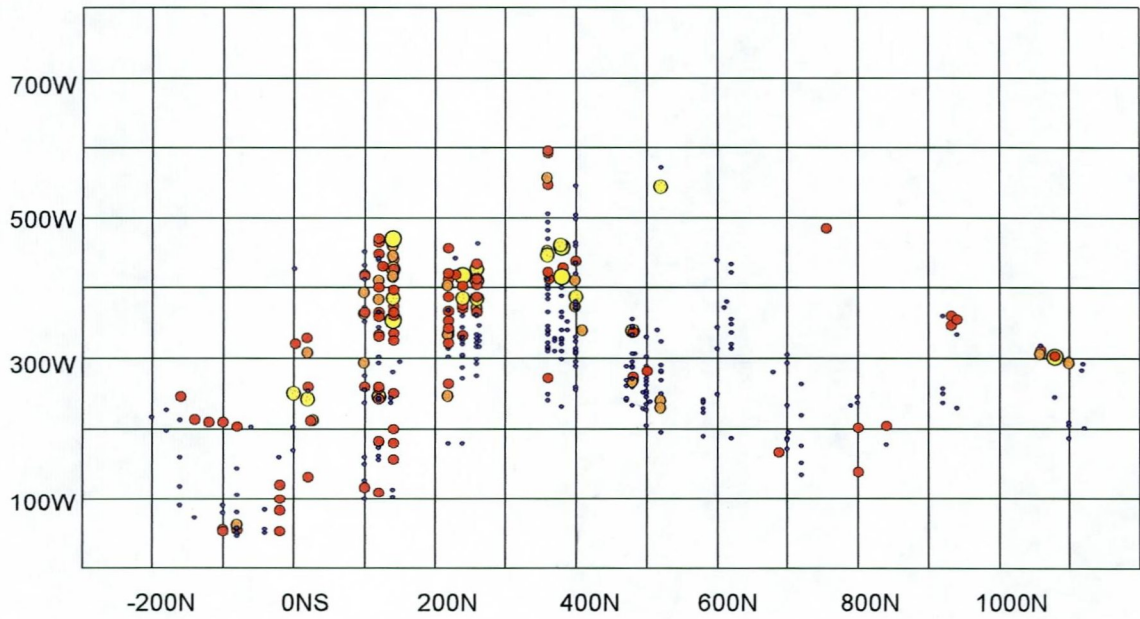
VMS type deposit (Kuroko model)



After Lydon 1984

Figure 4: Schematic models showing typical metal zonations in SEDEX-type and VMS-type sulfide deposits (After Large 1980 and Lydon 1984, respectively).

XY projection



XZ projection

m.a.s.l.

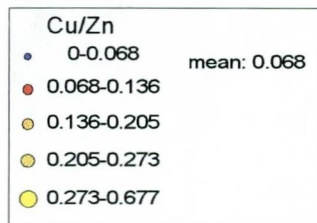
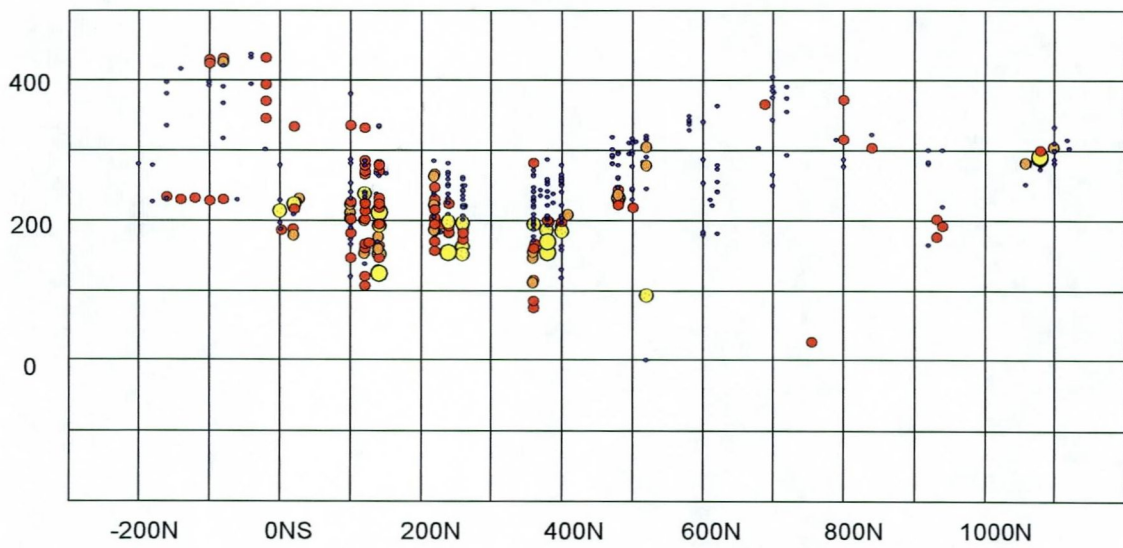


Figure 5: The Cu/Zn-ratio in drillhole intersections, shown in the XY (North vs. West) and XZ (North vs. Depth) projections. The symbols and values are according to standard deviations from the mean.

YZ projection

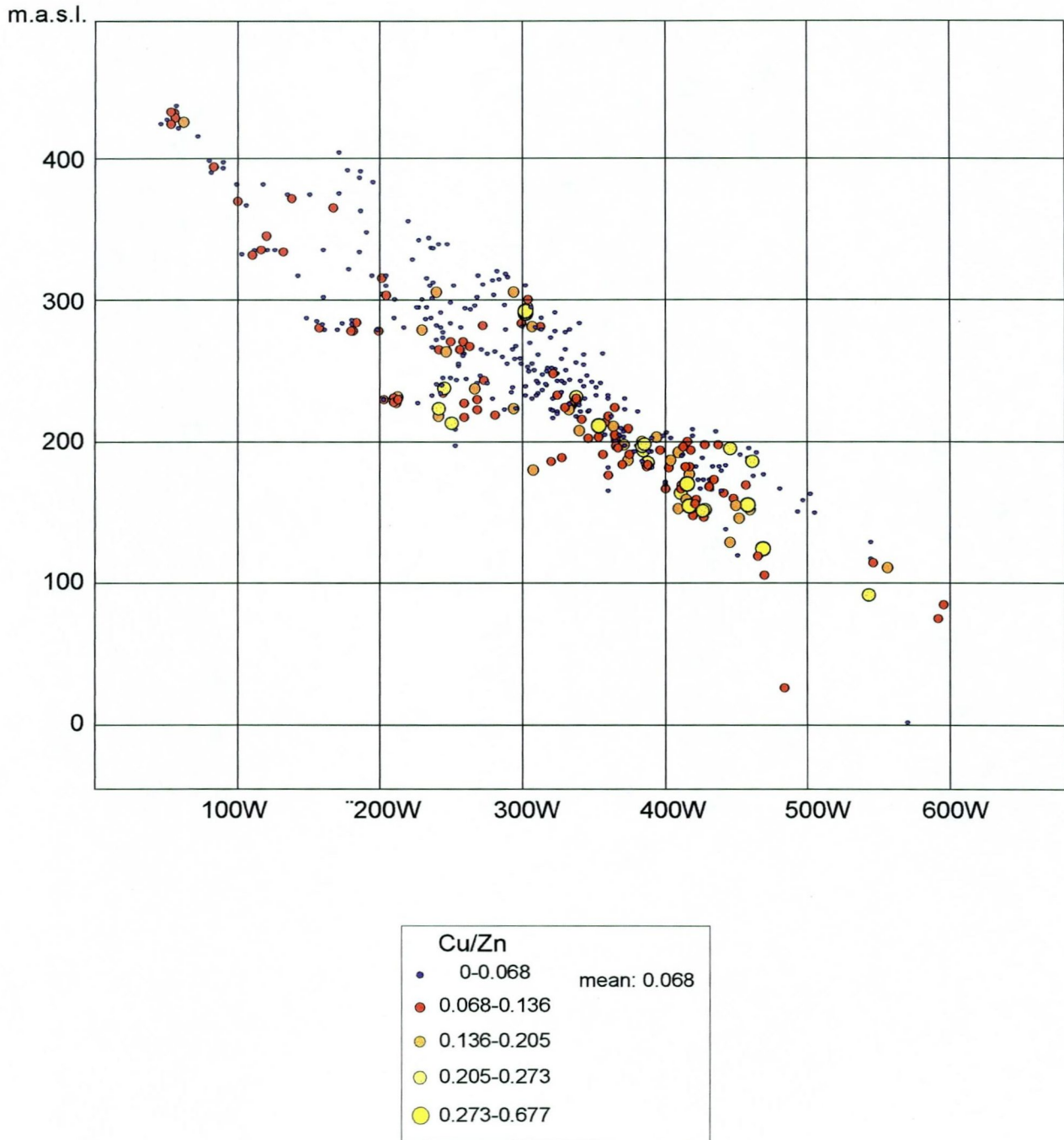


Figure 6: The Cu/Zn-ratio in drillhole intersections, shown in the YZ (West vs. Depth) projection. The symbols and values are according to standard deviations from the mean.

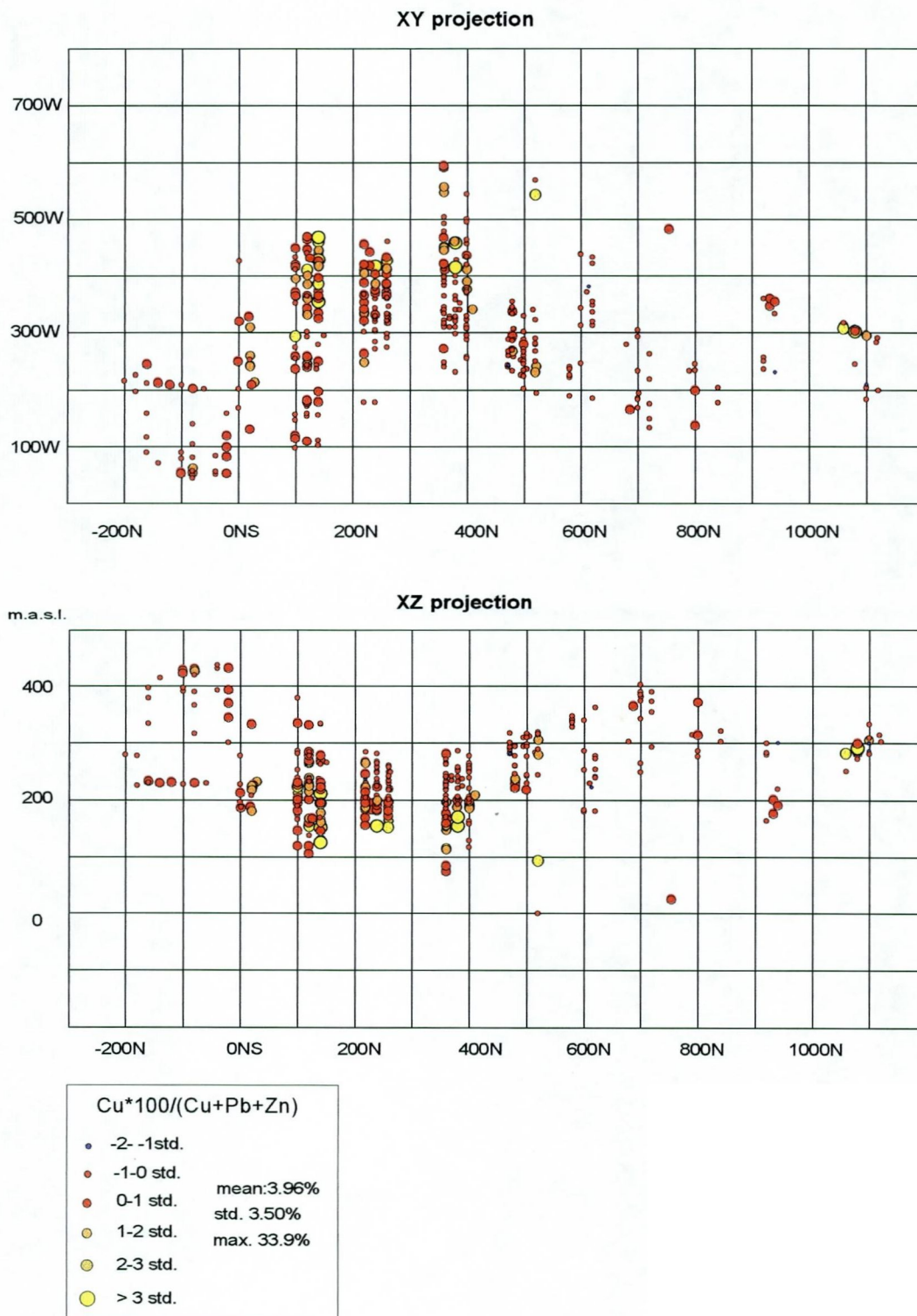


Figure 7: The Cu - percentage in drillhole intersections, shown in the XY (North vs. West) and XZ (North vs. Depth) projections. The symbols and values are according to standard deviations from the mean.

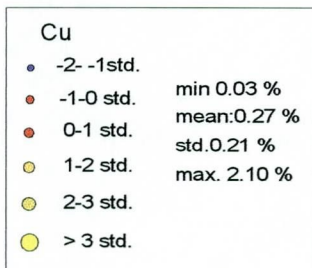
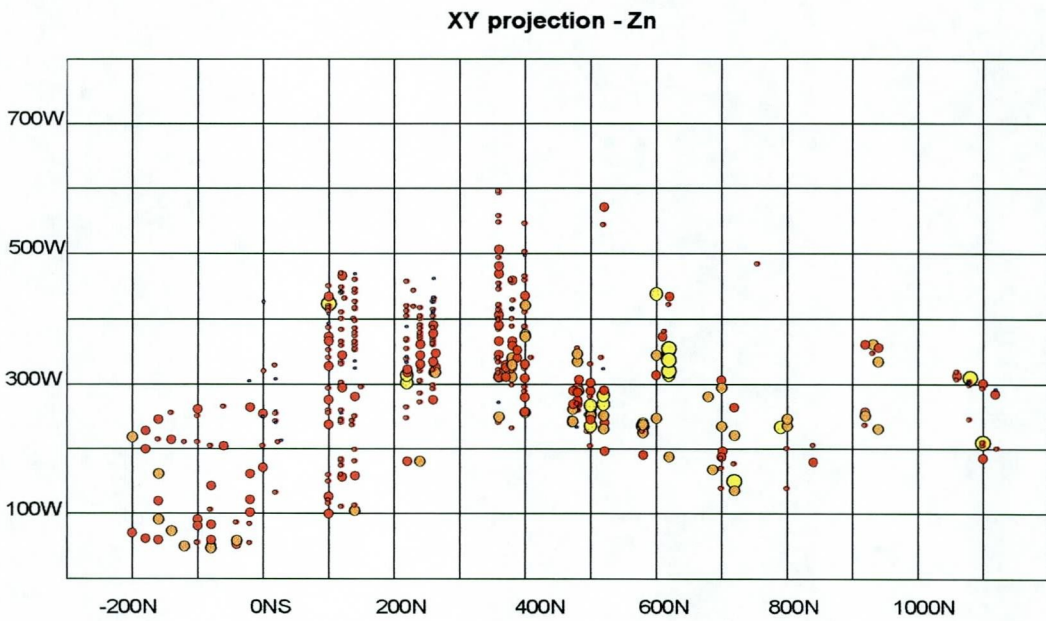
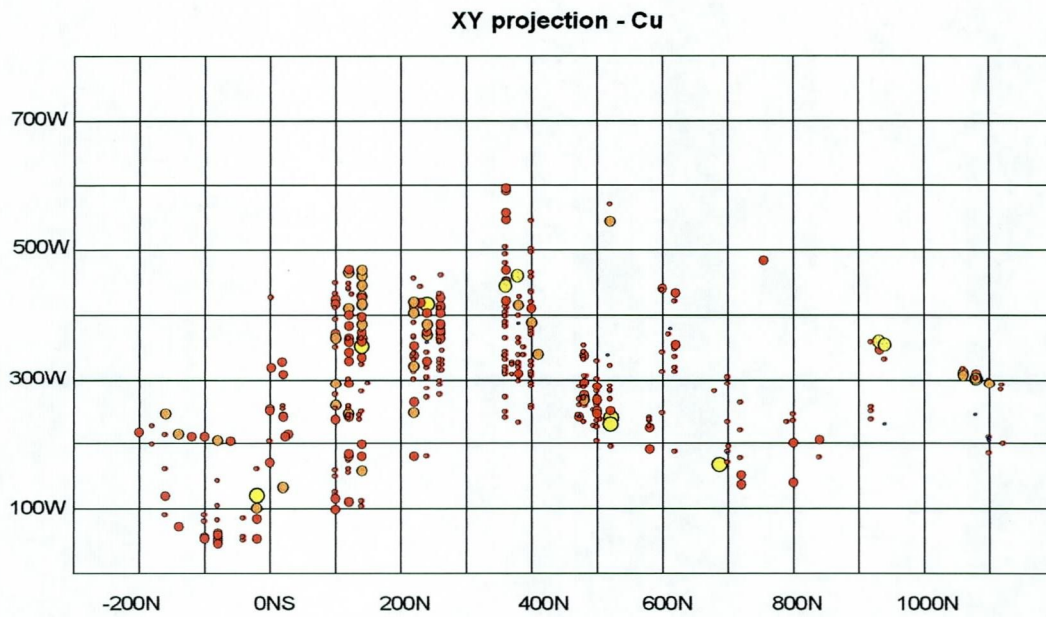
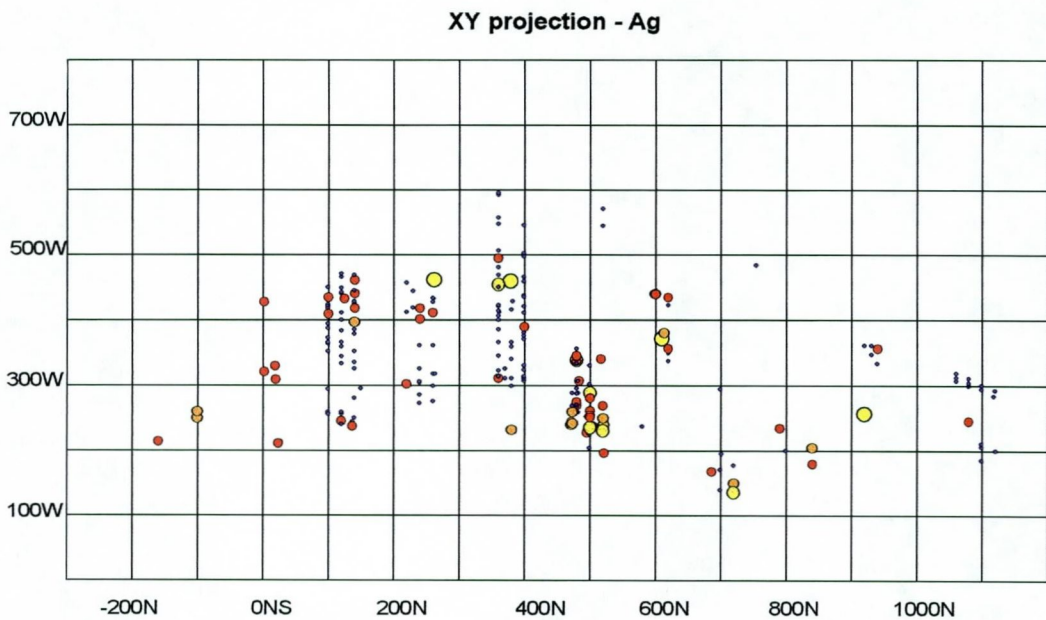
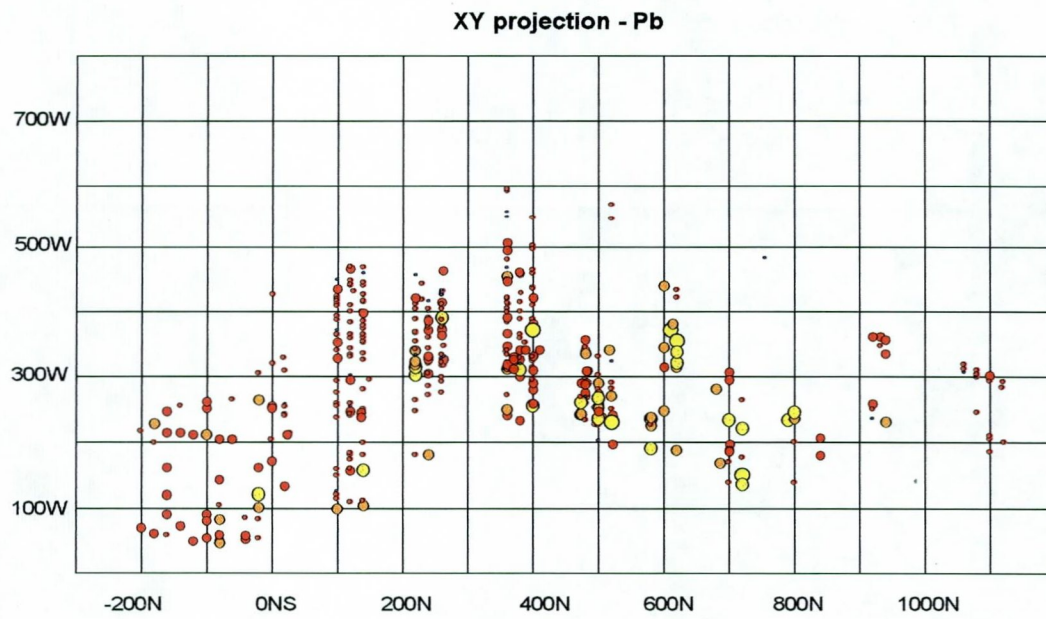


Figure 8: The Cu- and Zn-content in drillhole intersections, shown in the XY (North vs. West) projection. The symbols and values are according to standard deviations from the mean.



Pb	
• -2- -1std.	
• -1-0 std.	min. 0.12 %
• 0-1 std.	mean: 2.83 %
• 1-2 std.	std. 1.81 %
• 2-3 std.	max. 13.00 %
• > 3 std.	

Ag	
• -2- -1std.	
• -1-0 std.	min. 7.2 ppm
• 0-1 std.	mean: 53.7 ppm
• 1-2 std.	std. 54.9 ppm
• 2-3 std.	max. 471.3 ppm
• > 3 std.	

Figure 9: The Pb- and Ag-content in drillhole intersections, shown in the XY (North vs. West) projection. The symbols and values are according to standard deviations from the mean.

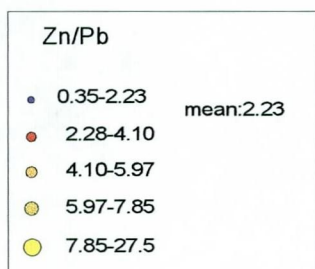
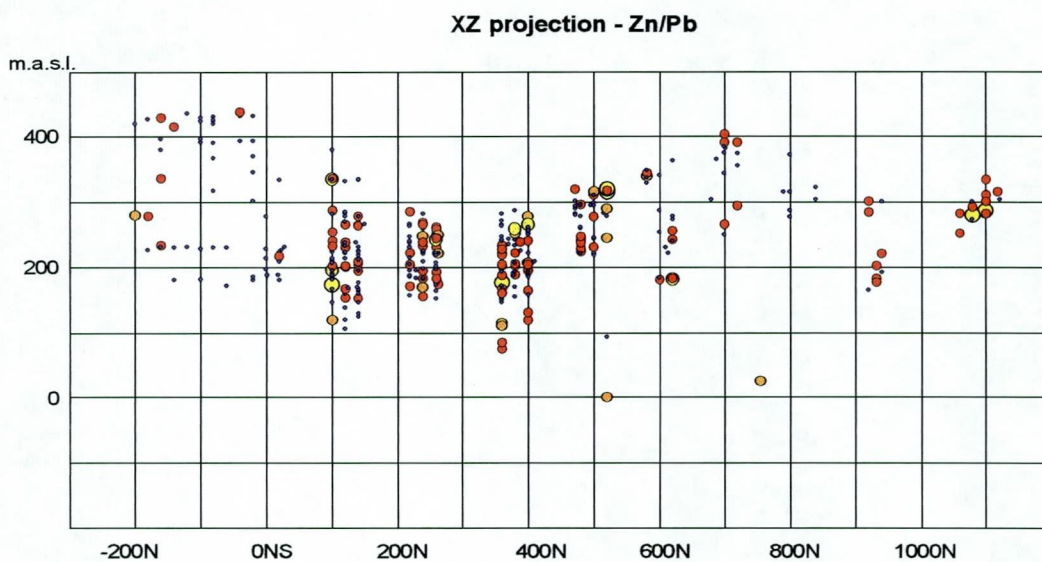
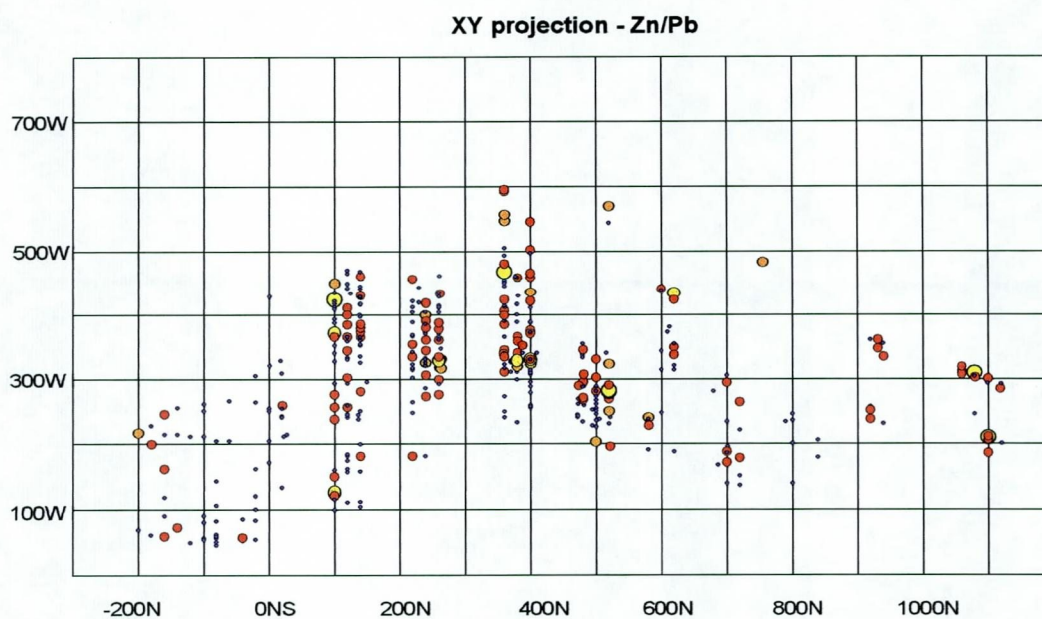


Figure 10: The Zn/Pb-ratio in drillholes, shown in the XY (North vs. West) and XZ (North vs. Depth) projections. The symbols and values are according to standard deviations from the mean.

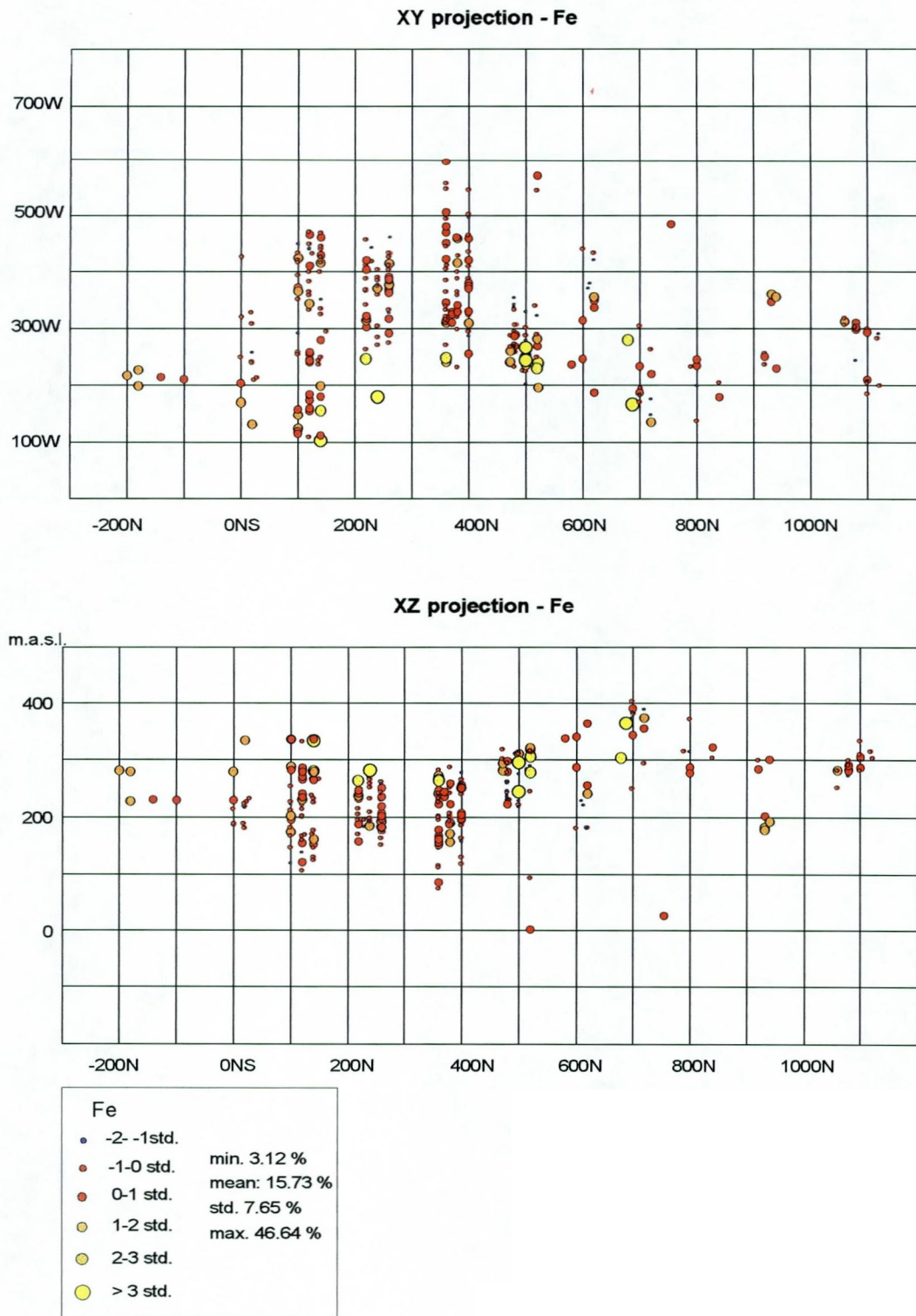


Figure 11: The Fe-content in drillhole intersections, shown in the XY (North vs. West) and XZ (North vs. Depth) projections. The symbols and values are according to standard deviations from the mean.

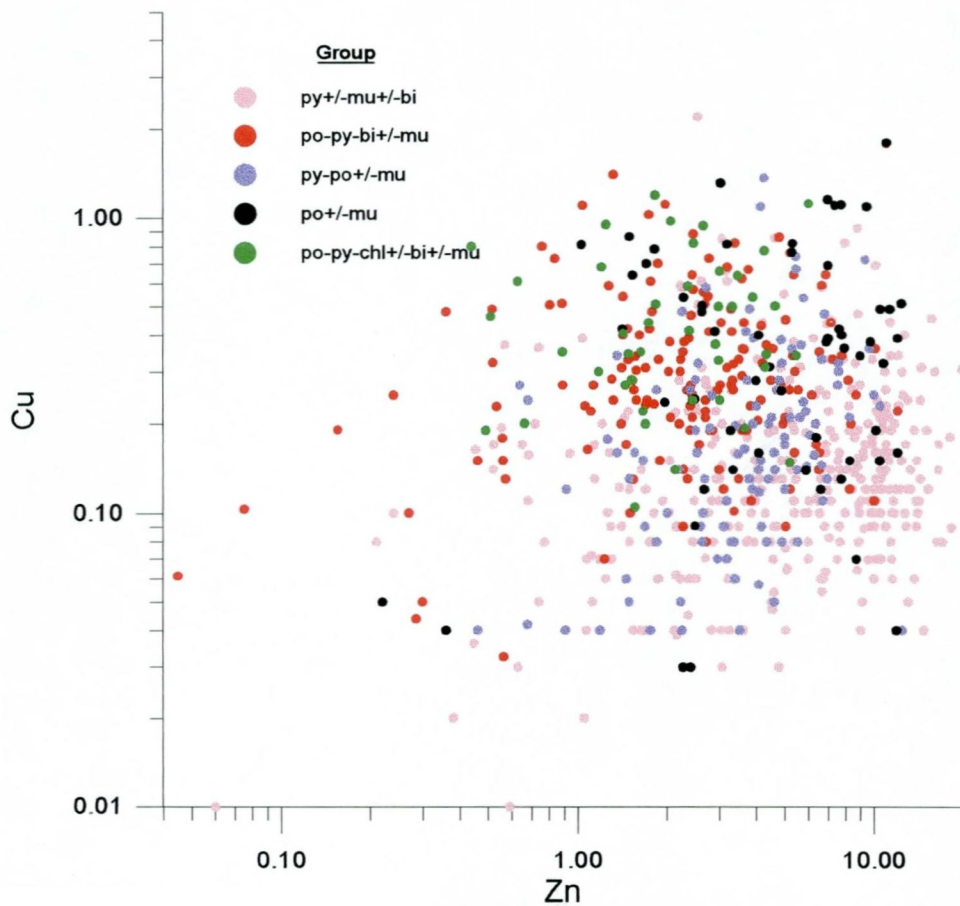
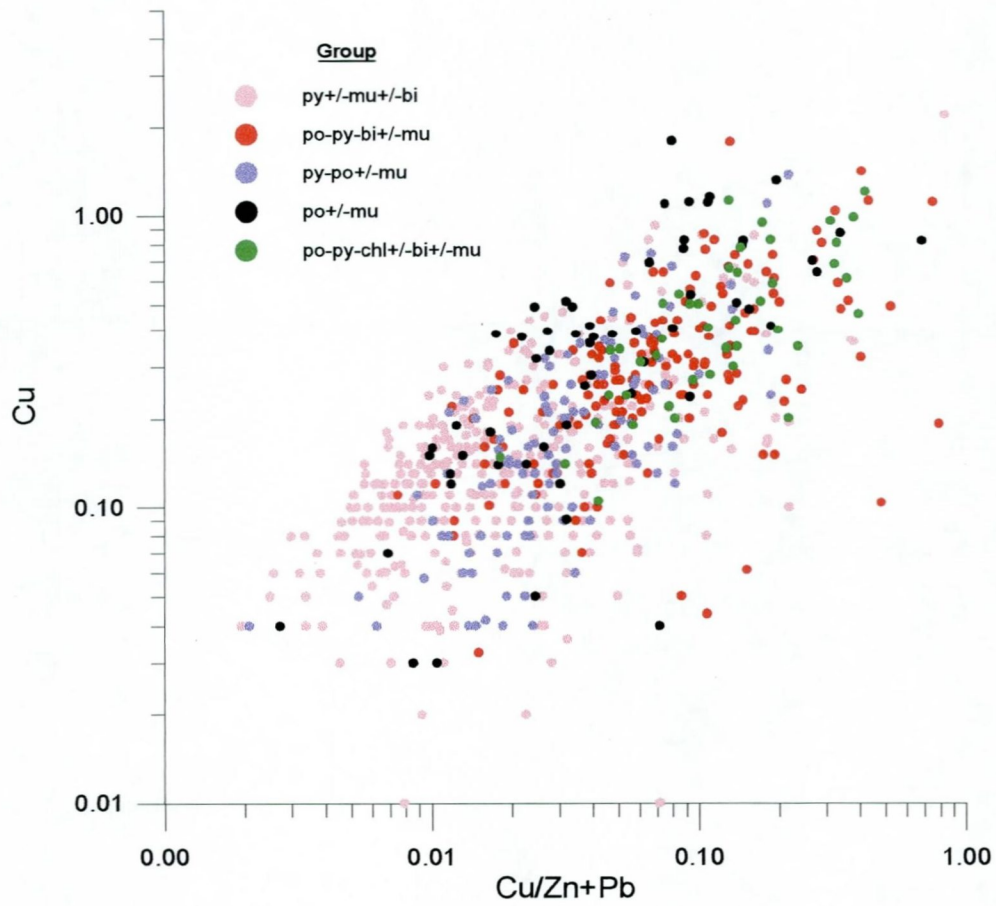
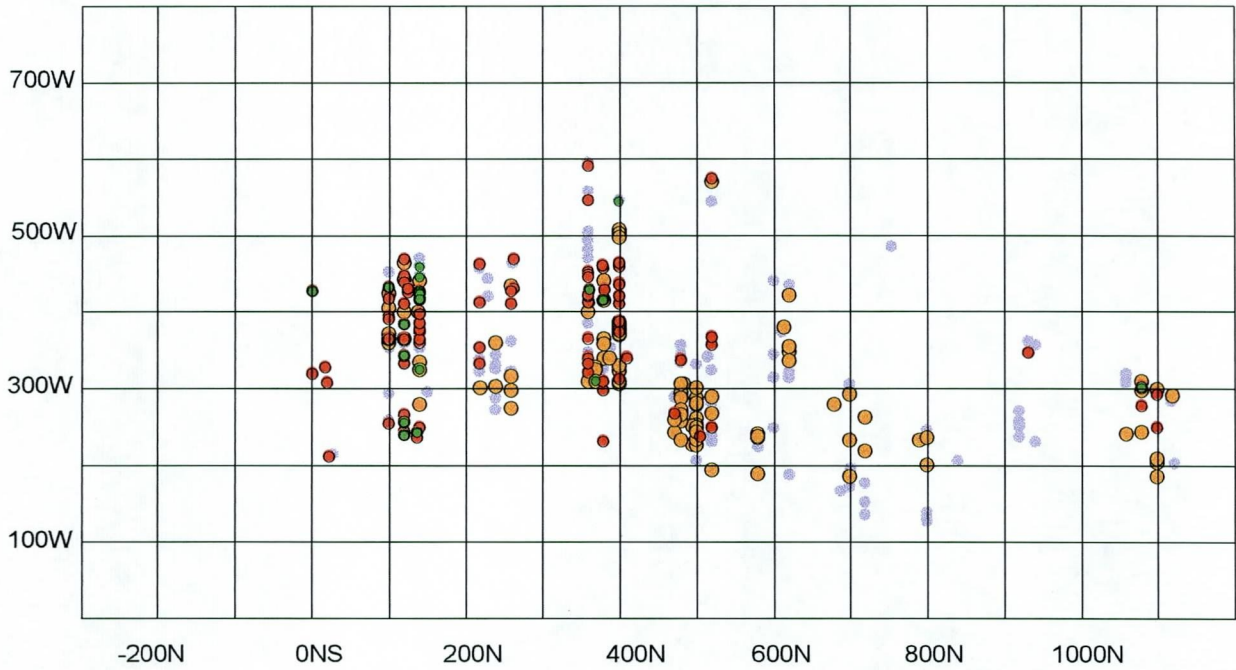
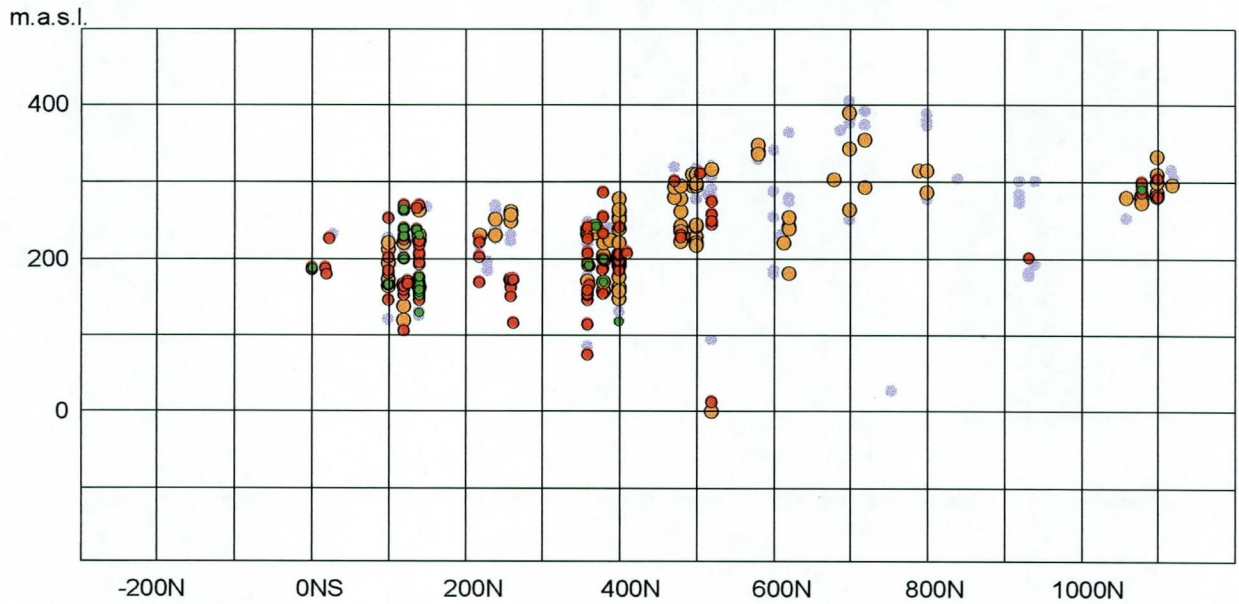


Figure 12: Plots of Cu-content versus the Cu/Zn+Pb-ratio and Cu-content versus Zn content in the individual analyzed core intervals and grouped according to mineral assemblages.

XY projection - Fe-sulfides and alteration minerals



XZ projection - Fe-sulfides and alteration minerals

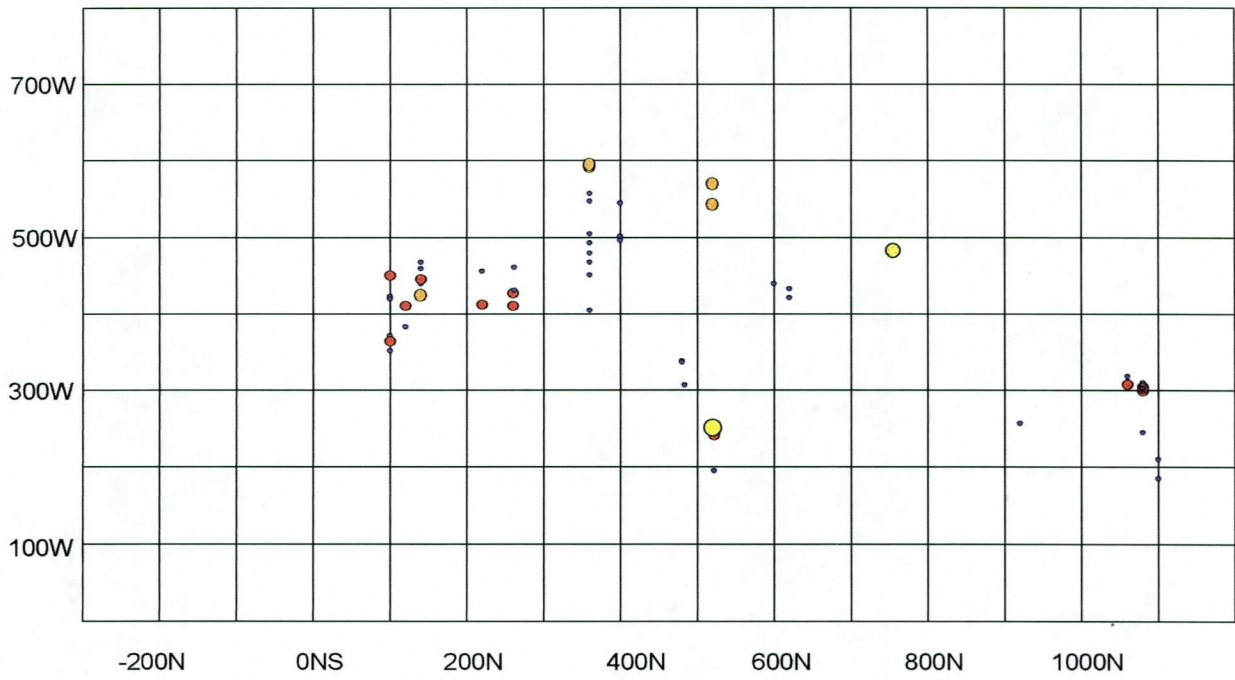


Mineral assemblages

- po-py-chl+/-bi+/-mu
- po-py-bi+/-mu
- py+/-mu+/-bi
- All described sections

Figure 13: The occurrence of various mineral assemblages in drillhole intersections, shown in the XY (North vs. West) and XZ (North vs. Depth) projections.

XY projection - Ba



XY projection - Mn

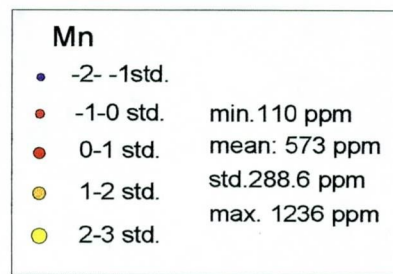
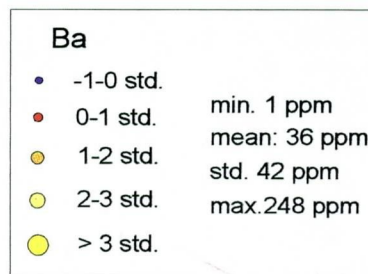
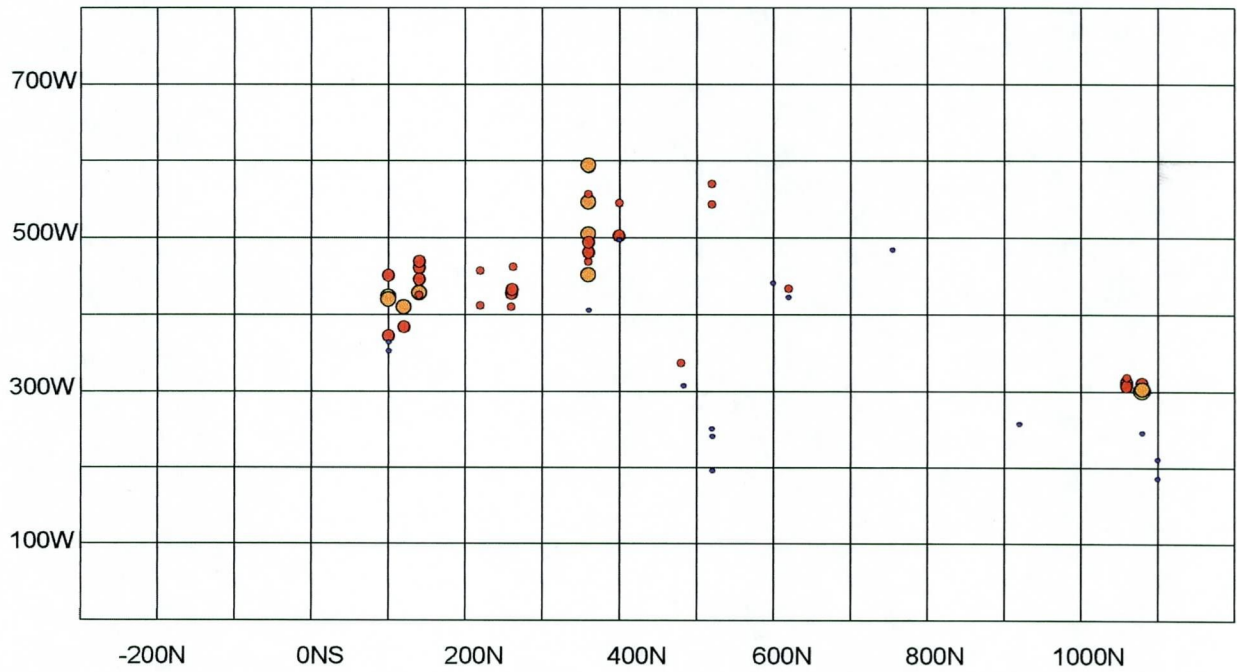


Figure 14: The Ba- and Mn-content in drillhole intersections, shown in the XY (North vs. West) projection. The symbols and values are according to standard deviations from the mean.

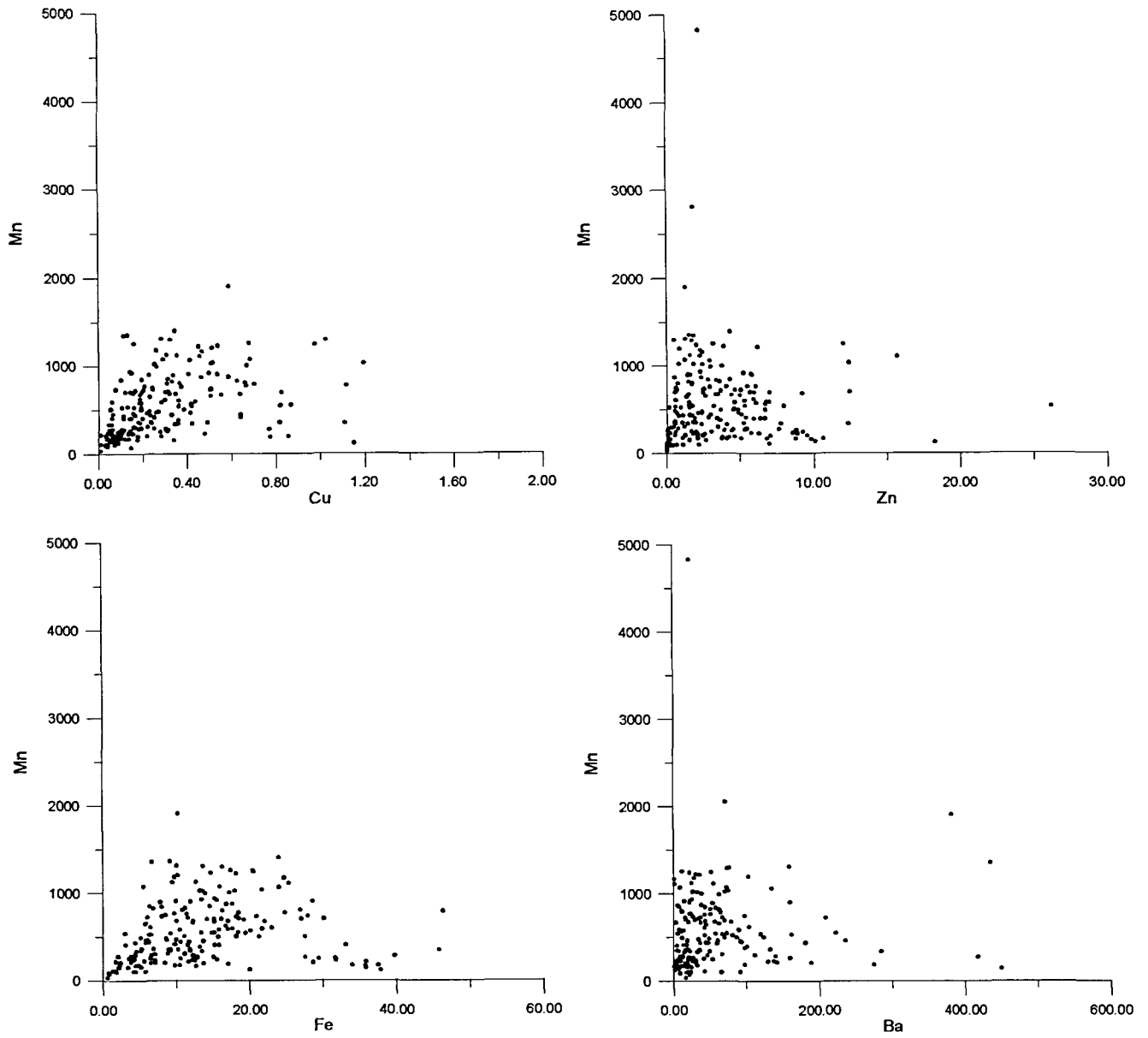


Figure 15: Plots of Mn-content versus Cu-, Zn-, Fe- and Ba-content for the ore intervals in the drillhole intersections (explanations in the text).

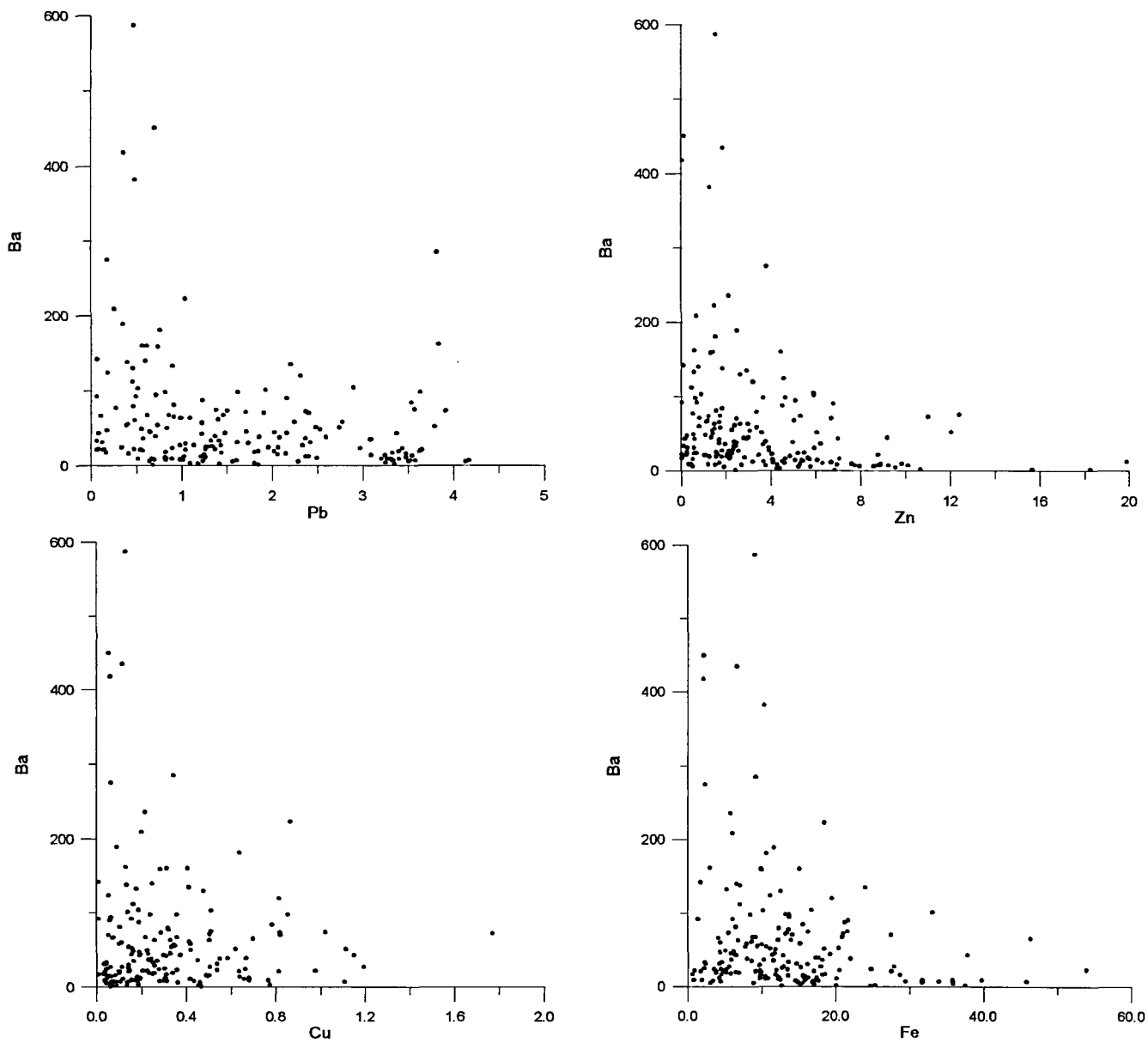


Figure 16: Plots of Ba-content versus Fe-content and versus content of base metals for the ore intervals in the drillhole intersections (explanations in the text).

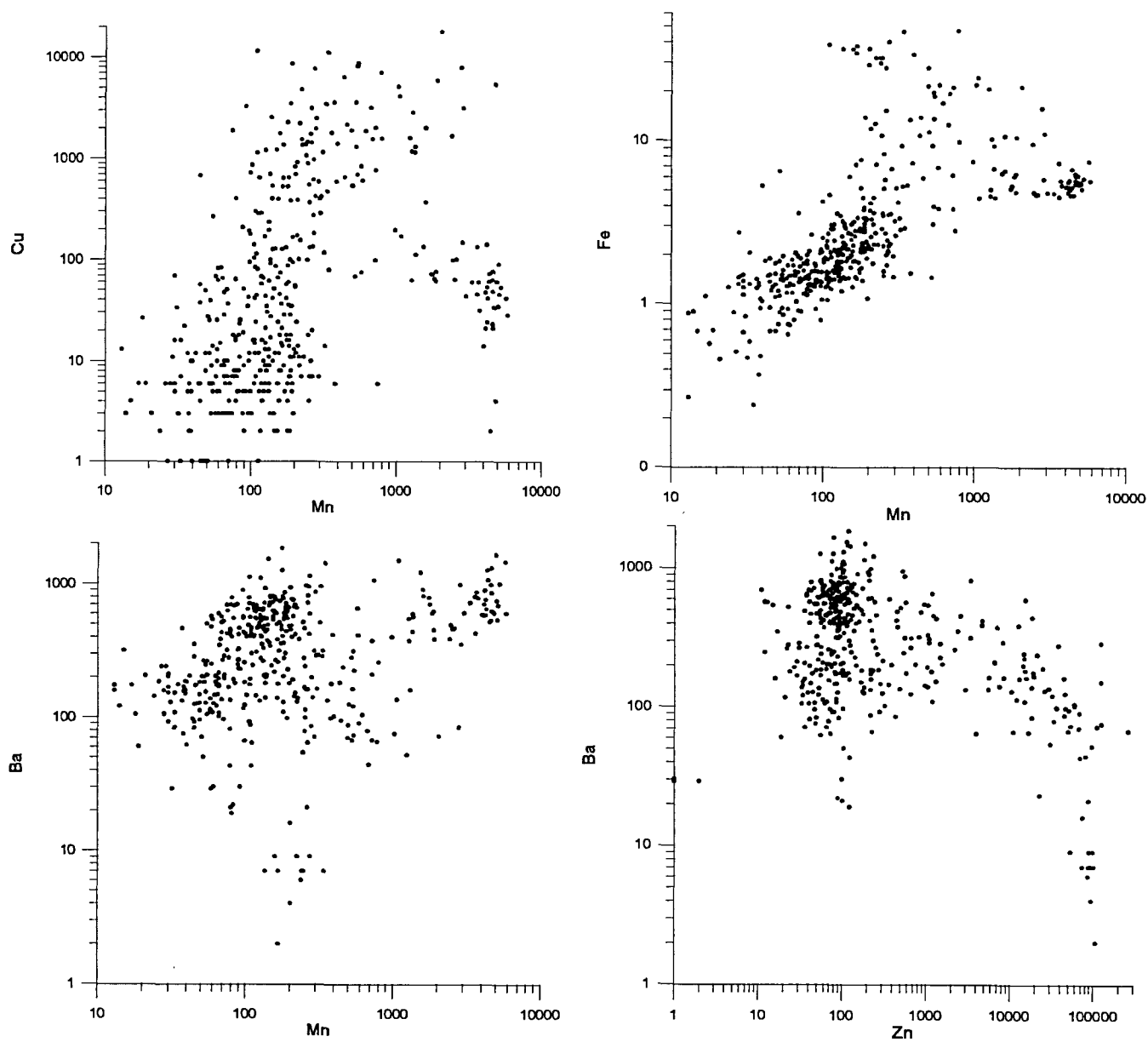


Figure 17: Plots of Mn-content versus Cu-, Fe- and Ba-content and of Ba-content versus Zn-content for ore, alteration and wall rock intersections in cores from profile 360 N (DH 2-90), 520 N (bh. 28-91, bh. 39-93, bh. 9-89, bh.24-91, DH 4-90 and DH 5-90) and 755 N (DH 1-90) (explanations in the text). Data from Moralev et al. 1995.

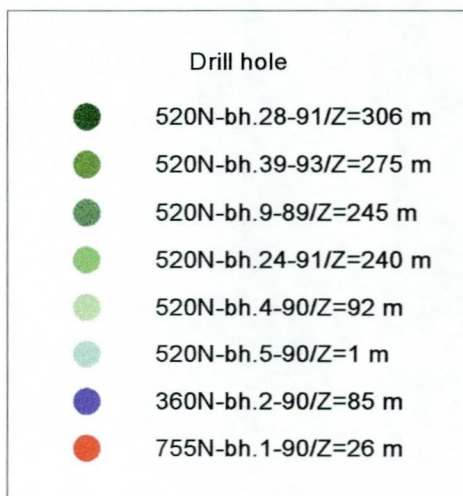
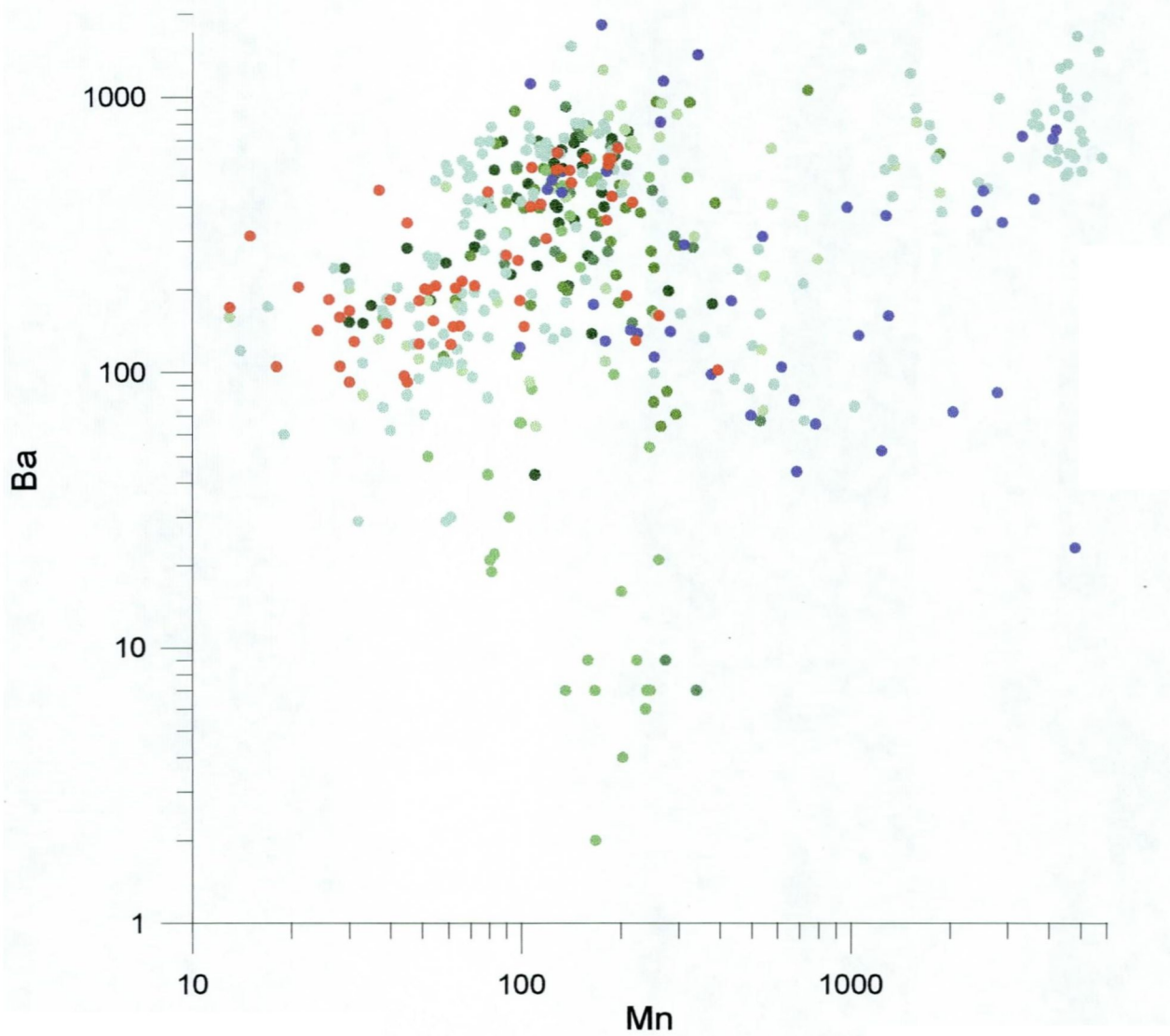


Figure 18: Ba-content versus Mn-content in drillholes from the profiles 360 N, 520 N and 755 N. The Z-values in the legend is the depth of ore intersections. Data from Moralev et al. 1995.

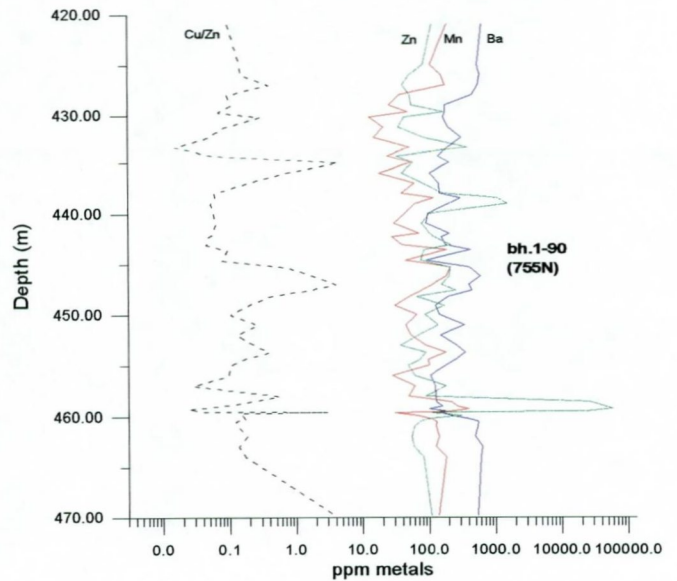
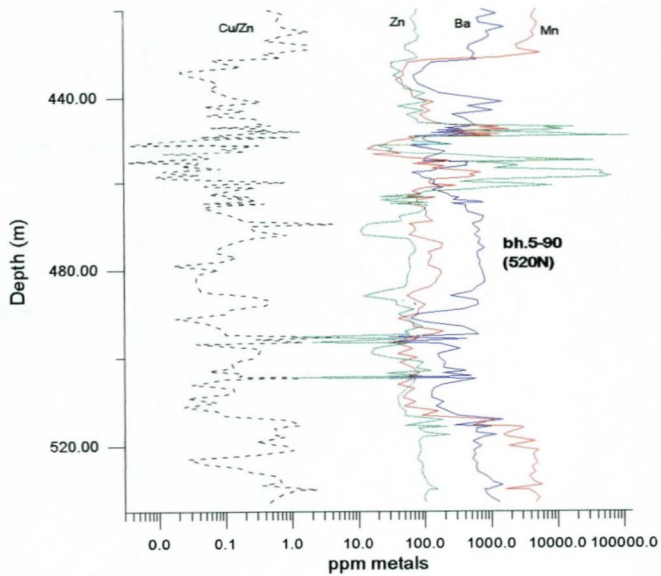
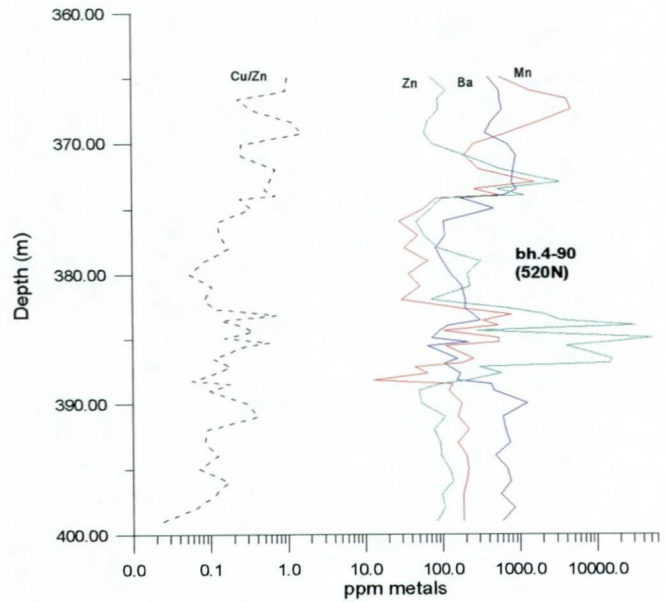
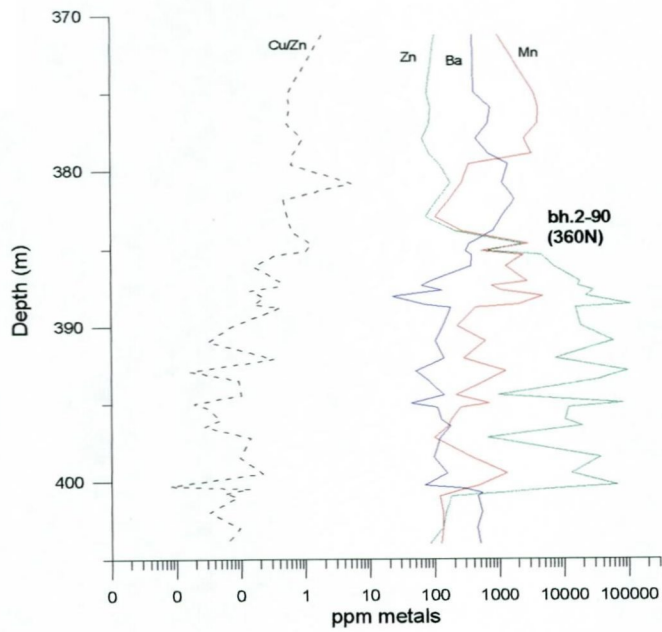


Figure 19: The content of Zn, Ba and Mn and the Cu/Zn-ratio plotted against depth in the drillholes 1-90, 2-90, 4-90 and 5-90. Data from Moralev et al. 1995.

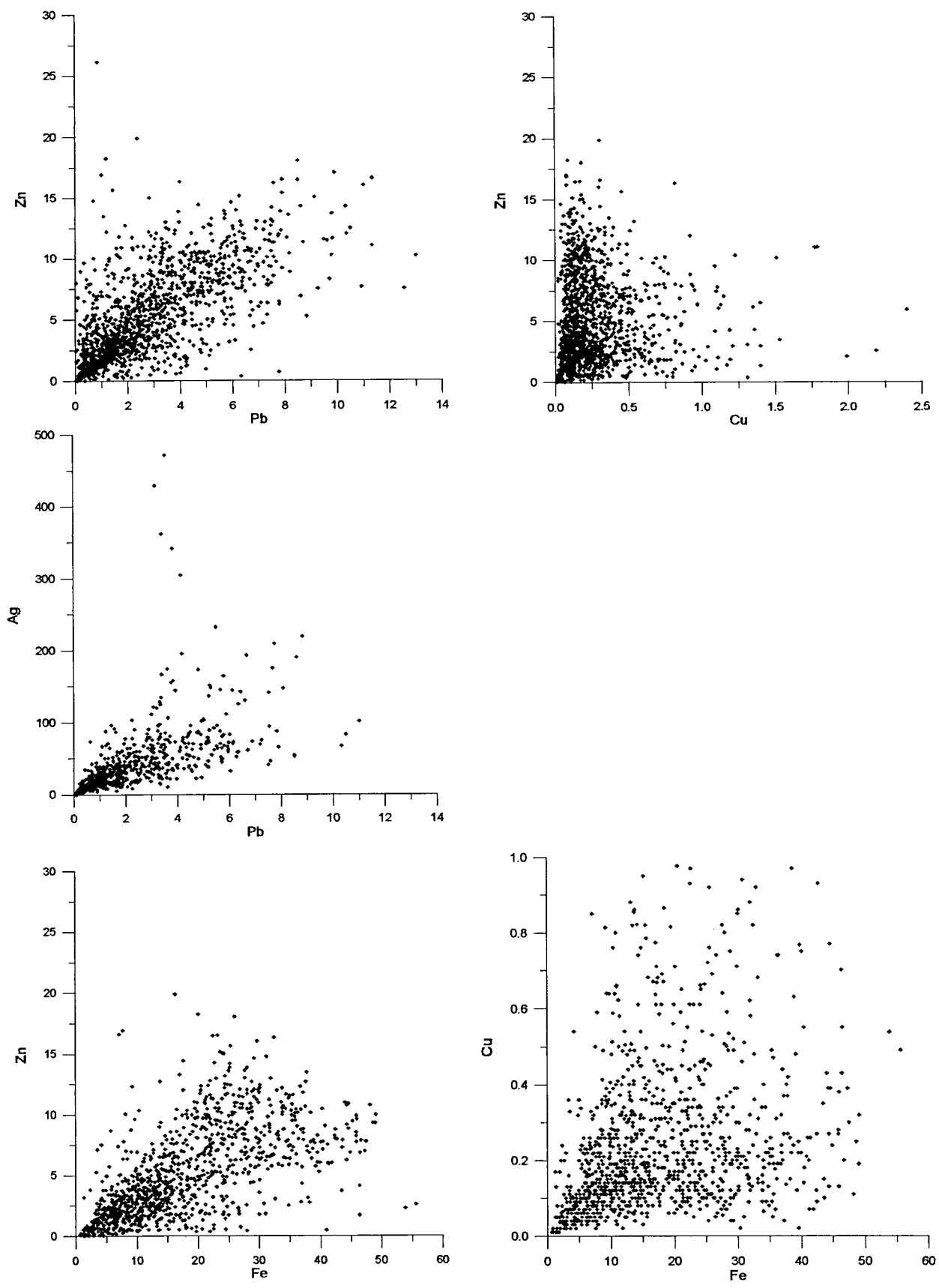


Figure 20: XY-plots for base metals, Fe and Ag, including all analyzed sections, in the drillholes (N= 1437). For explanations, see text.

Drillhole	year	Comments	X	Y	Z	meters	Cu	Pb	Zn	Ag	Au	Fe	S	Co	As	Cd	Sb	Bi	Ba	Mn
GH9+GH10	?		-40	51.5	432.5	8.29	0.26	3.69	7.47				33.56							
GH8	?	Hangingwall	-80	55	431.5	2.50	0.42	2.79	3.29				15.47							
GH7	?		-80	50.5	427	4.06	0.45	4.40	6.70				24.33							
GH7	?	Footwall	-80	46	423.5	1.35	0.45	4.90	9.76				29.15							
GH6	?		-100	56	428.5	1.10	0.39	2.24	3.91				12.90							
GH6	?	Footwall	-100	53	424	1.50	0.45	3.37	4.76				19.50							
GH3	?		-80	81.5	390	3.06	0.18	4.65	7.35				23.03							
GH2+GH4	?		-40	85	394	7.10	0.26	2.74	4.50				14.11							
GH14	?		-20	83	394	3.56	0.38	2.41	3.32				18.9							
GH13	?		-100	90	393	6.90	0.26	4.05	5.85											
GH12	?		-20	53	432.5	6	0.27	2.47	3.82				20.28							
GH10	?	Hangingwall	-40	56.5	437	1.23	0.21	3.23	8.86				26.32							
DH9B	?		-80	142.5	317	7.12	0.2	3.87	7.77				30.13							
DH8	?		-160	160	336	8.97	0.22	3.38	9.42				37.0							
DH5	?		-160	118	381	9.39	0.29	3.17	5.86				22.9							
DH4	?		-160	90	397	1.65	0.16	4.28	8.98				34.3							
DH3	?		-100	80	398	7.85	0.18	3.16	6.65				21.63							
DH28	?		0	253	197	3.05	0.34	3.59	5.77											
DH27	?	Hangingwall	-160	244.5	234	1.40	0.51	2.91	7.04				23.65							
DH25	?		-80	203	229.5	2.90	0.55	4.47	4.47				17.42							
DH21	?		-20	160	302	10.31	0.25	3.83	6.57				23.24							
DH2	?		-20	100	370	2.08	0.61	6.12	5.71				19.24							
DH16	?		100	99	381	0.70	0.34	5.56	7.08				25.41							
DH15	?		-140	72.5	415	2.10	0.31	3.67	8.58				37.7							
DH14	?	Hangingwall	-80	62	425	2.55	0.37	1.10	2.09				9.30							
DH14	?		-80	58	421	10.40	0.35	3.80	7.63				28.00							
DH10	?	?	-80	106	367		0.22	2.53	4.08				15.99							
DH1	?		-20	120	346	0.60	0.94	7.84	7.31				23.9							
bh.5-97	97	Hangingwall	400	497	158	14.40	0.07	1.70	1.99	45.5	326	5.03		8	326	50.9	292	10	26	261
bh.47-97	97		100	451	119.5	1.60	0.19	0.66	2.80	9.5	25	6.36		23	4732	92.1	13	18	44	844
bh.19-97	97	Hangingwall	400	545	117	41.10	0.24	1.58	4.57	18.8	82	15.40		52	349	56.5	194	61		483
bh.18-97	97	Hangingwall	400	507.5	147.5	5.20	0.19	0.34	0.56	19.6	567	15.17		20	400	150.0	480	50		700
bh.12-97	97	Hangingwall	400	501	147.5	4.80	0.36	0.21	0.74	15.6	142	26.88		30	400	210.0	110	50		800
bh.10-97	97		140	446	129	41.40	0.60	1.85	3.44	36.8	255	14.76		25	103	169.3	67	57	41	790
bh.9-96	96	Hangingwall	400	502	162.5	3.70	0.19	1.80	4.40	32.8	182	15.21		20	551	157.0	131	27	3	668
bh.8-96	96		120	410	153	3.60	0.67	1.37	3.76	17.8	436	17.28		40	1683	147.8	26	71	39	999
bh.4-96	96		100	405	164.5	2.95	0.33	1.09	1.48	14.5	203	6.88		9	77	62	27	7	63	818
bh.4-96	96	Hangingwall	100	423.5	173	0.30	0.45	1.42	15.65	24.4	169	25.34		93	344	501.5	16	54	2	1107
bh.3-96	96		100	419.5	147	3.65	0.18	1.52	2.35	17.1	71	12.79		20	174	92.6	27	30	30	863
bh.30-96	96		140	428	152	10.30	0.51	0.80	1.90	19.8	124	15.80		25	27	81.4	4	54	8	945
bh.30-96	96	Hangingwall	140	459.5	152	2.90	0.63	0.90	3.41	55.3	307	20.61		66	93	137.4	23	81	2	640

align!

Drillhole	year	Comments	X	Y	Z	meters	Cu	Pb	Zn	Ag	Au	Fe	S	Co	As	Cd	Sb	Bi	Ba	Mn
bh.29-96	96		140	424	155.5	4.80	0.41	0.61	1.43	13.7	86	9.94		9	24	52.3	17	39	160	904
bh.29-96	96	Hangingwall	140	441	163.5	2.90	0.23	1.81	2.32	55.8	190	14.22		47	101	105.5	59	71	21	403
bh.28-96	96	Hangingwall	1080	302.5	292	5.50	0.51	0.59	1.75	16.6	81	11.88		32	629	60.7	19	47	10	793
bh.27-96	96	Hangingwall	1080	304	300	4.60	0.22	1.05	2.08	28.6	85	10.39		14	542	78.8	41	41	27	944
bh.26-96	96	Hangingwall	1080	303.5	295	2.00	0.62	2.74	3.59	51.2	89	11.22		37	169	138.9	107	75	51	822
bh.25-96	96	Hangingwall	1080	302	290	6.50	0.82	1.65	2.65	35.6	84	16.32		34	247	104.5	44	111	65	1236
bh.25-96	96	Hangingwall	1080	309.5	280	0.55	0.31	2.37	19.88	42.5	220	16.29		48	562	636.9	168	41	12	794
bh.24-96	96	Hangingwall	1080	299	283	2.60	0.55	2.59	4.97	33.1	110	22.03		96	740	206.8	77	50	38	669
bh.21-96	96	Hangingwall	1080	278	287	1.00	0.51	0.51	0.89	15.6	24	10.23		14	32	22.7	1	60	103	1198
bh.21-96	96		1080	244.5	273	0.70	0.05	2.40	4.53	59.2	54	4.30		1	101	105.4	121	2	12	268
bh.10-96	96	Hangingwall	400	544.5	129	10.8	0.25	1.88	4.70	15.8	107	13.86		26	500	121.9	161	13	26	501
bh.30-95	95	Hangingwall	360	505	150	2.00	0.24	3.13	5.78	40.6	97	18.54		35	1153	224	267	68	10	905
bh.30-95	95	Hangingwall	360	493	150.5	1.05	0.16	3.09	3.66	63.5	193	11.59		16	325	146.9	193	34	35	715
bh.29-95	95	Hangingwall	360	480.5	167	1.10	0.14	1.73	5.93	15.4	39	16.16		34	271	188.2	94	7	30	700
bh.25-95	95		360	452	146	1.00	0.30	1.30	1.58	70.8	179	12.73		42	174	57.3	118	65	25	1121
bh.24-95	95		360	449	153	3.00	0.49	0.41	0.52	10.2	217	11.88		42	124	14.9	6	33	16	350
bh.24-95	95	Hangingwall	360	546.5	114.5	4.60	0.44	0.94	4.45	27.0	153	13.32		26	159	105.7	86	37	30	988
bh.24-95	95	Hangingwall	360	556	111	3.90	0.45	0.55	3.14	8.8	99	9.99		11	544	96.4	65	9	15	484
bh.19-95	95		600	439.5	179	0.65	0.30	3.20	7.61	119.7	761	12.50		18	3163	243.8	225	65	9	276
bh.84-94	94	Hangingwall	1060	318	252	2.10	0.26	2.02	4.85	20.2	151	10		11	86	134.8	45	35	19	463
bh.83-94	94	Hangingwall	1060	307	281	1.60	0.50	0.98	2.64	23.5	73	12.26		82	146	72.9	29	65	63	657
bh.83-94	94	Hangingwall	1060	312.5	281	2.20	0.66	2.06	5.47	38.8	151	24.8		201	252	158.9	82	56	24	769
bh.81-94	94	NE-profile	1060	241	279.5	5.00	0.04	0.67	0.45	32.4	221	1.9		1	1645	6.4	129	4	9	91
bh.80-94	94		1100	186	334	1.70	0.06	1.84	6.84	15.7	82	12.71		37	835	174.9	87	4	1	165
bh.77-94	94		1100	210	287	3.20	0.09	1.18	18.25	49.8	52	20.06		95	443	584.6	123	73	2	121
bh.76-94	94		1100	250	282	5.70	0.26	0.18	0.33	9.9	42	10.05		75	57	7.5	3	64	60	903
bh.6-94	94	Hangingwall	480	337.5	228	1.30	0.23	1.85	1.81	60.3	178	6.92		3	45	48.9	186	39	19	356
bh.5-94	94	Hangingwall	480	338	231.5	2.15	0.34	3.39	1.56	166.3	808	5.23		6	1949	48.8	2449	147	19	151
bh.4-94	94		483.5	307	230	1.20	0.06	3.24	5.08	88.1	250	10.47		27	233	161.5	143	70	14	173
bh.26-94	94	Hangingwall	360	404.5	202	3.00	0.16	2.49	6.29	47.0	147	12.23		39	276	119.6	135	41	10	230
bh.15-94	94		220	412	169	6.00	0.31	2.37	2.73	47.7	318	8.67		14	40	74.7	101	43	37	533
bh.15-94	94	Hangingwall	220	456.5	169	2.40	0.25	0.82	2.84	10.8	41	9.89		9	219	64.6	75	7	18	411
bh.15-94	94	Hangingwall	220	463	169	2.55	0.16	2.53	1.08	59.5	472	6.26		7	1780	18.9	769	37	48	432
bh.12-94	94		380	440.5	158	0.60	0.16	3.14	0.94	428.7	1763	6.34		12	108	70.9	1061	480	34	522
bh.10-94	94	Hangingwall	100	365	221	8.40	0.16	0.58	0.93	11.2	65	7.28		9	57	21.8	25	17	94	368
bh.10-94	94	Hangingwall	100	360	214	2.10	0.12	0.84	1.38	25.3	103	8.43		14	96	56.9	21	28	59	322
Bh.39-93	93	Hangingwall	520	357	258	1.90	0.06	0.13	0.23	5.0	64	4.15		8	101	7.1	9	9	28	242
Bh.39-93	93	Hangingwall	520	357	274.5	0.90	0.03	1.61	0.56	86.5	40	2.40		2	26	28.2	189	43	31	206
bh.3-93	93	Hangingwall	261	462	175	1.20	0.06	4.14	1.92	304.7	178	3.12		3	298	81.2	740	119	5	403
bh.34-93	93		100	372	195.5	2.40	0.44	0.98	6.94	25.4		17.65		48	151	182.6	39	31	8	589
bh.30-93	93		620	422	182	7.10	0.08	1.22	3.31	22.5		4.03		4	906	75.7	59	4	7	158

Drillhole	year	Comments	X	Y	Z	meters	Cu	Pb	Zn	Ag	Au	Fe	S	Co	As	Cd	Sb	Bi	Ba	Mn
bh.1803-74	74	Hangingwall	260	384.5	197	8.30	0.41	3.31	1.95			20.91								
bh.1803-74	74	Hangingwall	260	391	202	0.85	0.07	6.91	5.97			19.55								
bh.1802-74	74		240	370.5	183.5	3.00	0.54	3.46	5.10			24.92								
bh.1801-74+1	74		240	375	191	6.55	0.32	2.25	4.42			15.53								
bh.1801-74	74		240	379	193	3.55	0.14	1.23	3.84			7.60								
bh.1801-74	74	Hangingwall	240	386	198	6.10	0.58	3.20	2.69			13.95								
bh.3307-73	73		120	110	332	5.80	0.30	2.17	2.41			13.72								
bh.3306-73	73		100	126	335.5	2.60	0.13	0.75	5.58			25.68								
bh.3305-73+b	73		100	121	335.5	11.60	0.23	1.29	3.68			19.40								
bh.3305-73	73		100	116	335.5	6.10	0.32	1.99	4.26			21.14								
bh.2804-73	73		100	149	287	13.05	0.19	1.85	4.15			24.53								
bh.2803-73	73		100	159.5	282.5	22.40	0.18	1.79	3.8			19.81								
bh.2302-73	73	Hangingwall	220	263	267	4.85	0.33	1.45	2.88			10.19								
bh.2301-73	73	Hangingwall	220	247	263	1.5	0.49	1.49	3.31			33.74								
bh.1807-73	73		220	445	139	1.90	0.24	0.58	0.94			7.07								
bh.1806-73	73		220	421	155.5	1.07	0.51	3.07	4.43			21.88								
bh.1804-73	73		380	401	181.5	2.25	0.87	1.34	1.21			23.87								
bh.1803-73	73		380	389	193	6.55	0.04	1.53	3.35			15.69								
bh.1803-73	73	Hangingwall	380	401	206	4.50	0.08	1.77	2.36			10.73								
bh.1812-72	72		260	387	182	1.49	0.28	1.80	4.03			17.62								
bh.1809-72	72		220	388	184	6.00	0.24	2.04	2.08			13.76								
bh.1809-72	72	Hangingwall	220	404	187	4.60	0.51	2.82	3.43			21.89								
bh.1808-72	72		220	367	195.5	4.60	0.21	1.29	2.78			13.16								
bh.1808-72	72	Hangingwall	220	368	204.5	5.35	0.1	2.15	3.45			8.96								
bh.1806-72	72	?	-20	263	180	1		4.7	6.36											
bh.1806-72	72	?	-20	305	185	4		1.2	2											
bh.1805-72	72	?	-100	250	181	2		2.9	4.3	117										
bh.1805-72	72	? Hangingwall	-100	260	181	1		3.4	7.2	130										
bh.1804-72	72	?	-140	256	180	0.5		1.6	3.0											
bh.1803-72	72	?	100	386.5	188	1.5		2.6	3.5	42										
bh.1803-72	72	? Hangingwall	100	408	194.5	3		1.3	2.1	58										
bh.1802-72	72	?	100	341	206	5.5		2.2	3.4											
bh.1801-72	72	?	100	327.5	213	1		3.2	6											
bh.1501-72	72	?	-60	265.5	172	1		2.1	2.3											
bh.2503-71	71	Footwall	400	289	254.5	2.40	0.09	3.52	2.45			7.21								
bh.2502-71	71		400	294.5	257.5	8.30	0.11	2.29	3.66			15.54								
bh.2501-71	71		400	308.5	250	5.40	0.19	3.02	6.55			26.64								
bh.2501-71	71	Hangingwall	400	331	250	18.00	0.08	2.71	5.74			17.28								
DH2-70	70	Hangingwall	520	367	250.5	2.20	0.05	0.28	0.30			4.17								
DH1-70	70	Hangingwall	360	341	242	5.10	0.25	2.45	5.14			11.09	13.02							
DH1-70	70		360	333	226	23.50	0.22	1.35	4.14			14.71	16.79							

